JGR Atmospheres

RESEARCH ARTICLE
10.1029/2021JD035905

Topographic Influences on Diurnally Driven MJO Rainfall Over the Maritime Continent

Hedanqiu Bai[1] and **Courtney Schumacher**[1]

[1]Department of Atmospheric Sciences, Texas A&M University, College Station, TX, USA

Key Points:

- The first harmonic and the time of maximum hourly rain rate produce different diurnal rain patterns over the Maritime Continent
- Daily and diurnal rain anomalies during the Madden-Julian Oscillation (MJO) are asymmetrical around topography with similar convective and stratiform rain contributions
- The asymmetry of rainfall around topography is determined by convergence by MJO-scale winds while MJO moisture plays less of a role

Correspondence to:
H. Bai,
baisy@tamu.edu

Citation:
Bai, H., & Schumacher, C. (2022). Topographic influences on diurnally driven MJO rainfall over the Maritime Continent. *Journal of Geophysical Research: Atmospheres*, *127*, e2021JD035905. https://doi.org/10.1029/2021JD035905

Received 24 SEP 2021
Accepted 28 FEB 2022

Abstract This work investigates impacts of the Madden-Julian Oscillation (MJO) on the daily and diurnal rainfall over the Maritime Continent, with emphasis on the influences of topography over Sumatra, Borneo and New Guinea. Eighty-nine MJO events were identified during 2001–2019 using IMERG satellite data. Daily and diurnal rainfall maxima on the east side of topography lag the west side as the MJO passes. In addition, the island vanguard (pre-MJO) rain is more convective, while the island rearguard (behind the main MJO body) rain is more stratiform. The timing and magnitude of diurnal rainfall is defined using the maximum hourly rain rate instead of the first diurnal harmonic to avoid smoothing. While a single sharp peak is observed over the mountains around 19 LT, a much broader delayed peak occurs over land to the west of topography and two peaks are observed over land to the east of topography at 15 and 2 LT. Rain peaks offshore from 3 to 7 LT. Cluster analysis shows that the afternoon and nighttime rainfall peaks are highest before the MJO arrives, then gradually decrease and become earlier on the west side of the topography, whereas the afternoon (nighttime) peak east of the topography is enhanced before (after) the MJO arrives. The contrasting east-west features can be attributed to topographic influences on the moisture flux convergence of the mean column moisture by MJO-induced winds. The MJO wind modulation of diurnal rainfall over most of the open ocean areas is insignificant.

Plain Language Summary The Indo-Pacific Maritime Continent (MC) has complex geography and strong variations in rainfall throughout the day. The Madden-Julian Oscillation (MJO) is a slow, eastward-moving envelope of storminess in the tropics, initiating over the Indian Ocean and propagating across the MC into the West Pacific over a month's time. The passage of the MJO can strongly impact when and how much it rains over the MC islands. Using a 19-year satellite data set, we show that higher rain amounts occur on the west side of the mountains before the east side as the MJO passes. There is also a strong dependence when rain occurs during the day on whether you are to the west, over, or to the east of the mountains when the MJO passes. The east-west rainfall differences can be attributed to the influence of the mountains on the mean moisture distribution and MJO-induced winds. This study highlights the role of mountains in modulating the impacts of the MJO on rainfall over the MC islands, and thus the importance of accurately representing topographic effects in numerical models.

1. Introduction

Located in the Indo-Pacific warm pool, the Maritime Continent (MC) has complex geography and a strong diurnal cycle in convection and rainfall. While land convection peaks during the day, precipitation over the ocean usually peaks in the evening to the early morning (e.g., Hirose et al., 2008; Nesbitt & Zipser, 2003). Over the coastal ocean, the afternoon deep convection propagates offshore at night, leading to a nocturnal rainfall maximum up to hundreds of kilometers offshore (e.g., Biasutti et al., 2012; Kikuchi & Wang, 2008; Yang & Slingo, 2001). Different sizes, elevations and orographic orientations of the islands further add to the complexity of the precipitation distribution and atmospheric circulations over the MC (Rauniyar & Walsh, 2011; Sakaeda et al., 2020).

The Madden-Julian Oscillation (MJO; Jiang et al., 2020; Madden & Julian, 1972; Zhang, 2005) is a slow, eastward-moving large-scale convective envelope in the tropics, initiating over the Indian Ocean and propagating into the West Pacific on the time scale of 30–90 days. It is a dominant component of tropical intraseasonal variability bridging the gap between weather and climate (Zhang, 2013) and has significant impacts on the tropics and extratropics (e.g., McPhaden et al., 2006; Stan et al., 2017; Zhou et al., 2020).

The MJO interacts strongly with the MC as it passes over. Previous studies have shown that the MJO can modulate the precipitation distribution and diurnal cycle over the MC. Using infrared cloud observations from the

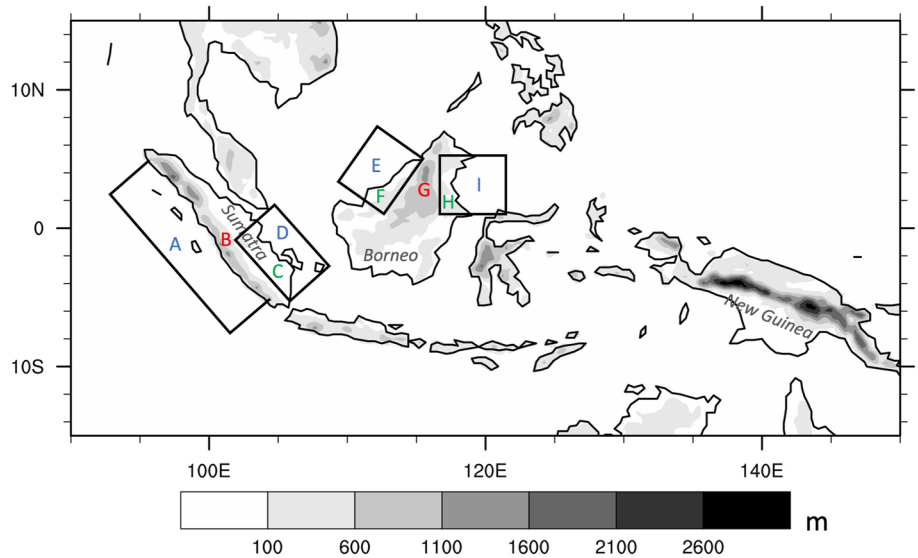

Figure 1. Topography of the Maritime Continent. Black boxes are used to show regional diurnal rainfall variations in Figure 8. Letters in blue, red and green indicate offshore, mountainous and low-elevation land regions, respectively. Coastlines are used to separate land and sea.

International Satellite Cloud Climatology Project and precipitation from the Tropical Rainfall Measuring Mission (TRMM) 3B42 product, Tian et al. (2006) found that the diurnal amplitude of deep convective cloud amount increases (decreases) over both land and water during the active (suppressed) MJO, but the diurnal phase is not significantly affected. However, Rauniyar and Walsh (2011) reported that rainfall during the active (suppressed) MJO peaks two hours later (earlier) than the diurnal cycle of climatological rainfall in DJF using TRMM 3B42 and 3G68 rainfall. Utilizing similar satellite rainfall observations, Peatman et al. (2014) found that the diurnal amplitude over land changes up to 10 mm/day between the active and suppressed phases of the MJO, and peaks 6 days before the active MJO reaches the MC. Birch et al. (2016) further attributed the earlier peak of the land convection to strong mesoscale circulations resulting from intense land surface insolation before the MJO arrives at the MC.

Orography and convection over the MC islands also impact the passage of the MJO. Numerous studies have investigated the "barrier effect" of the MC islands on the propagation of the MJO. While some studies (e.g., Inness & Slingo, 2006; Wu & Hsu, 2009) suggest that the orography of the MC islands can block the MJO, Zhang and Ling (2017) hypothesized that the diurnal convection over land may also act as a barrier. Ling et al. (2019) further proposed that a reduced diurnal amplitude of land convection helps the MJO to cross the MC. Taking out the diurnal cycle of the incoming solar radiation in a cloud-permitting regional model, Hagos et al. (2016) found that MJO convection strengthened as it moved across the MC. By changing the updraft plume radius over the MC land in a global climate model, Ahn et al. (2020) reported that the eastward propagation of the MJO is enhanced (reduced) when convective tops are shallower (deeper). Jiang et al. (2019) used ERA5 reanalysis to show that the MC topography and its associated diurnal cycle are essential to the low-level moisture advection by the MJO winds, thus regulating the passage of the MJO across the MC.

In this study, we will investigate impacts of the MJO on the MC daily and diurnal rainfall, with a particular focus on influences from the MC topography (Figure 1). We will look into convective and stratiform decomposition of the earlier peak of the land rainfall reported by Peatman et al. (2014), because it is important to indicate potential different organizations of the MJO over land and sea. This study will use the latest Integrated Multi-satellitE Retrievals for Global Precipitation Measurement (GPM) with much higher temporal and spatial resolutions compared to its predecessor. In addition, while most studies define the diurnal cycle as the first diurnal harmonic (e.g., Birch et al., 2016; Nesbitt & Zipser, 2003; Peatman et al., 2014; Seiki et al., 2021; Yang & Slingo, 2001), convective growth is often more of an instantaneous pulse than a sinusoidal oscillation. We would like to explore whether diurnal rainfall changes with the MJO are sensitive to different diurnal definitions. Furthermore, utilizing high-resolution reanalysis data, we will quantify the role of moisture and winds in MJO-induced rainfall,

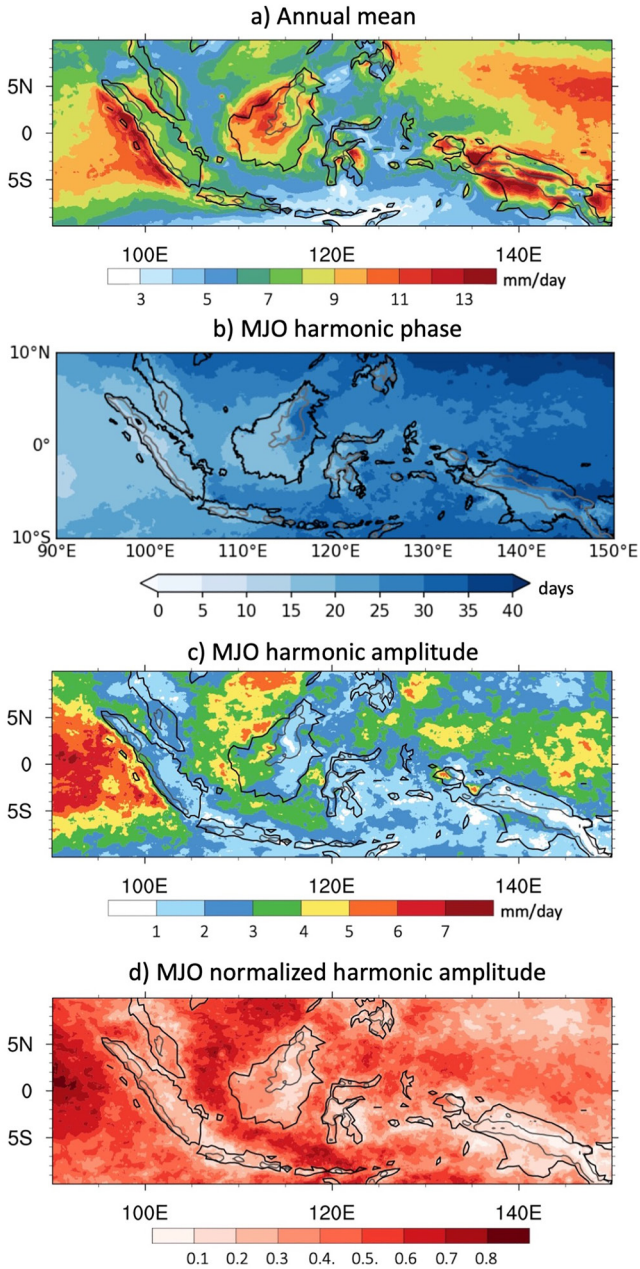

Figure 2. (a) IMERG annual precipitation climatology for 2001–2019. (b) Phase and (c) amplitude of the Madden-Julian Oscillation (MJO) harmonic for daily rainfall. (d) Amplitude of the MJO daily rainfall harmonic normalized by the precipitation climatology in (a). Elevation at 500 m is indicated with gray contours in all four maps.

and further explore interaction between the MJO and the MC topography. We will mainly focus on three major MC islands: Sumatra, Borneo and New Guinea. Data sources are described in Section 2. Topographic influences on the MJO-induced daily and diurnal rainfall variations are investigated in Section 3. Section 4 discusses the relationship of the MC diurnal rainfall with moisture and wind anomalies associated with the MJO. Finally, a summary and conclusions are given in Section 5.

2. Data and Methods

Nineteen years (2001–2019) of GPM product (IMERG version 06, Huffman et al., 2015) were used as the main precipitation data set in this study. IMERG fuses the precipitation estimates during the operation of the TRMM satellite with more recent (since 2014) precipitation estimates during GPM operations. The spatial resolution of IMERG is 0.1° and the temporal resolution is 30 min. The 30-min rain rate was averaged into hourly data to investigate characteristics of the diurnal rainfall. The high horizontal and temporal resolution data set enables us to look into detailed features of the rainfall variations over the MC island topography.

To investigate the partition of the total rainfall into convective and stratiform components, TRMM precipitation radar (PR) 2A23 data and GPM dual-frequency precipitation radar (DPR) 2ADPR data (Iguchi, 2020) were averaged into daily, 0.5° grids for 2001–2019. The TRMM 2A23 legacy data set was processed using the DPR algorithm. Only near-surface reflectivity greater than 18 dBZ was used given the lower sensitivity of the PR compared to DPR, which is sensitive down to about 14 dBZ. Wind and specific humidity for 2001–2019 from the fifth generation ECMWF atmospheric reanalysis ERA5 (Hersbach et al., 2020) were used to examine moisture and circulation features across the islands as the MJO passes. ERA5 has a spatial resolution of 0.25° and a temporal resolution of 1 hr.

MJO events were identified as follows: the 30-min IMERG precipitation was averaged into daily data, and an MJO wave number-frequency filter (eastward wave numbers 0–9 and period 30–96 days) was applied to the daily precipitation following Kiladis et al. (2005). Using different MJO filters do not change the overall results. The filtered precipitation was then averaged between 10°S and 10°N to identify the MJO. The standard deviation of MJO-filtered rainfall between 10°S and 10°N over the Indian Ocean-MC was estimated to be roughly 2.5 mm/day, consistent with the typical MJO rainfall perturbation of 3 mm/day found in Jiang et al. (2019). Active MJO envelopes were identified as MJO-filtered rainfall over 2.5 mm/day. Days with the maximum precipitation perturbation in the active MJO envelope at 90°E were taken as day 0. The MJO entering the MC must then propagate continuously to at least 105°E. A total of 89 MJO events were identified during the 19 years.

3. Topographic Influences on MJO-Induced Rainfall Variations

3.1. Daily Rainfall Variations

3.1.1. Total Rain

Figure 2a shows the IMERG climatological precipitation over the MC for 2001–2019. Large annual precipitation values (i.e., >10 mm/d or 3.6 m/yr) are found over the West Pacific warm pool, as well as to the west of the MC

mountains. Precipitation maxima west of the orography are related to mean winds converging at the base of the mountains (shown later in Figure 10a). Annual precipitation amounts are about two-thirds of the above values east of the mountains and about half over the interior seas.

To investigate impacts of the topography on the MJO-induced daily rainfall over the MC, the time series of the IMERG daily rainfall anomaly for the 89 MJO events at each grid point within 10°S-10°N, 90–150°E was Fourier fitted with the MJO harmonic. The period was chosen to be 44 days, consistent with the period of the maximum power of the MJO in Wheeler and Hendon (2004). Results are not sensitive to the choice of different periods within the range of the MJO spectral peak of 40–50 days. The MJO at 90°E is taken as day 0. An example time series of the daily rainfall anomaly and the fitted MJO harmonic is shown in the bottom panel of Figure 9a. Because the active and suppressed phases of the MJO are relatively symmetric, the fitted harmonic gives a reasonable approximation of the peak date and amplitude of the daily rainfall caused by the MJO across the MC (Figures 2b and 2c). The same Fourier fit method will be used later to examine diurnal rainfall variations under the influence of the MJO.

Over the MC islands, rainfall on the west side of the topography peaks about a week earlier (i.e., lighter shading) than the surrounding ocean (Figure 2b), consistent with Peatman et al. (2014). In contrast, the east side is roughly in phase with or slightly lagging the surrounding ocean except Sumatra, which will be discussed in detail in Section 4. Over much of the ocean and on the west side of the mountains, the MJO-induced rainfall variation is large (Figure 2c); however, smaller rainfall variations occur to the east of the mountains. To give a better sense of the MJO-induced daily rain relative to climatology, Figure 2d shows the MJO harmonic amplitude normalized by the annual mean precipitation in Figure 2a. While the climatological precipitation is larger over the islands compared to the interior seas, the largest MJO-induced rainfall variances are over the water, consistent with previous studies (e.g., DeMott et al., 2018; Peatman et al., 2014; Sobel et al., 2010; Zhang & Ling, 2017). The east-west land contrast in the MJO harmonic amplitude can still be observed in Figure 2d, but is not as distinct as the land-sea contrast.

Figure 3 shows lag days of the daily rainfall anomalies for the 89 MJO events compared to climatology, with the MJO at 90°E taken as day 0. On day −10 for Sumatra and day −5 for Borneo and New Guinea, the west side of the mountains on the islands and the region just offshore start to show positive daily rainfall anomalies, consistent with the "vanguard" of precipitation over land jumping ahead of the main body MJO reported by Peatman et al. (2014). The anomalous daily rainfall is either zero or slightly negative on the east side of Sumatra, Borneo and New Guinea, indicating that the vanguard rainfall only appears on the west side of the islands. On day −5 (Sumatra), day 0 (Borneo) and day 5 (New Guinea), the positive anomalies become larger on the west side of the islands. Anomalies also become positive over eastern Sumatra, but with a smaller amplitude compared to the ocean west of Sumatra. Positive anomalies on the east side of Borneo and New Guinea don't occur until days 5 and 10, respectively, because of their location further east. In addition, Borneo shows the strongest positive-negative contrast between the west and east sides of the mountains.

By day 5 (top right panel of Figure 3), the main body of the MJO is well over the MC, with an overall enhanced daily rainfall over both land and ocean. However, the offshore region west of Sumatra starts to show a slightly reduced daily rainfall as the MJO continues to move eastward. On days 10–15, when the suppressed MJO is over the western MC, the daily rainfall over land sees almost the opposite sign as days −5–0. A similar switch in sign occurs over Borneo, but with a smaller magnitude. A detailed analysis on moisture and wind will be given in Section 4 to explain the asymmetry.

3.1.2. Convective and Stratiform Rain

Mesoscale convective systems have been shown to contain significant contributions from both convective and stratiform rain over the West Pacific warm pool (Yuter & Houze, 1998) and the relative contribution of the stratiform rainfall to the total rainfall is a potential indicator of convective sustainability and mesoscale organization (Schumacher & Houze, 2003). Because IMERG does not differentiate between convective and stratiform rain types, we use radar observations from the TRMM and GPM satellites to investigate the geographical variation in convective and stratiform rain with the MJO over the MC. Figures 4a and 4b are the 19-year climatology of the convective and stratiform precipitation based on TRMM/GPM radar data. While there are roughly equal amounts of convective and stratiform rain over much of the MC domain, Sumatra, Malaysia, and Java have much lower stratiform rain contributions compared to other MC islands, potentially creating a barrier for the evolution

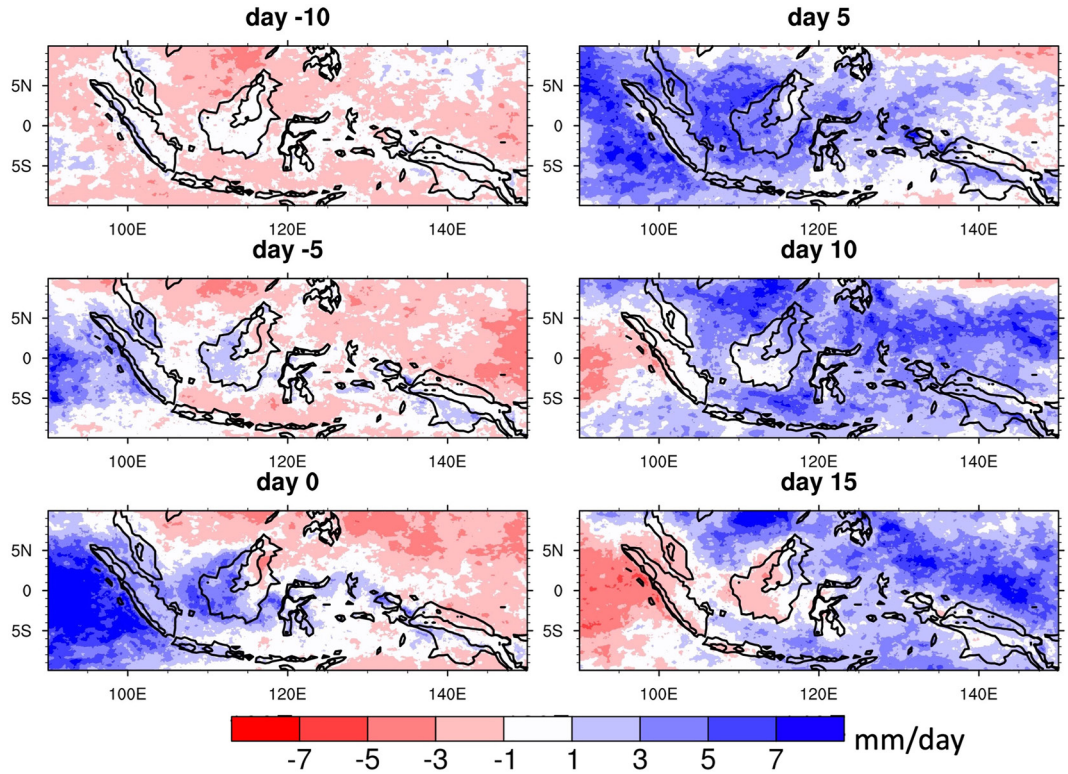

Figure 3. Lag days of the IMERG daily rainfall anomalies for the 89 Madden-Julian Oscillation events compared to climatology. Each panel is a 5-day average centered at the day indicated in the title. Elevation at 500 m is indicated with black contours.

of organized convective systems as the MJO approaches from the Indian Ocean. We also note possible quality issues with the PR/DPR observations over the steepest terrain (i.e., within the 500-m contour line), either due to misclassification by the rain type algorithm or because of the underestimation of PR/DPR shallow precipitation in mountainous regions (Arulraj & Barros, 2021; Duan et al., 2015). For example, there is an abrupt shift from high to low convective rain amounts over the New Guinea ridge line, with stratiform rain showing the opposite signal. This switch may be due to algorithm issues rather than indicating a true physical pattern.

Figures 4c and 4d show lag days of daily convective and stratiform rain anomalies compared to climatology as the MJO passes, with the MJO at 90°E as day 0. Because of the sparse and discontinuous nature of the radar data samples, each panel is a 9-day average of the day range indicated in the title. On day −15–−7, representing the inactive MJO, convective rain increases slightly over Sumatra and Borneo due to enhanced clear-sky insolation. However, enhanced stratiform rain is not observed over the islands. The main body of the MJO consists of a large fraction of stratiform rain (seen mainly over the ocean and inner Indonesian seas) because there are more organized convective systems inside the MJO (e.g., Virts & Houze, 2015). The enhanced stratiform rain follows the propagation of the MJO over the MC from day −6 to day 20, with larger anomalies than the convective rain. Similar to days −5 and 0 in Figure 3, the east-west rainfall asymmetry is seen in both convective and stratiform rain on day −6–2 over the topography of Sumatra, Borneo and New Guinea when the active MJO just arrives at the MC. On day 3–11, Sumatra and Borneo start to see negative convective rain anomalies but stratiform anomalies remain positive over the islands. We term this the "rearguard", that is, the attempt to keep rain from decreasing over the islands. As the suppressed phase approaches on day 12–20, the east-west rainfall asymmetry is present again over Borneo (albeit flipped from day −6 to 2) and negative convective (but not stratiform) anomalies appear over New Guinea. The results indicate that the vanguard of precipitation over land reported by Peatman et al. (2014) is a "convective vanguard" and that positive stratiform rain anomalies persist longer than the positive convective anomalies over the MC islands as the MJO exits (i.e., the "stratiform rearguard"). These findings are also consistent with Zhang et al. (2010) and Barnes et al. (2015) who showed that the shallow component of the

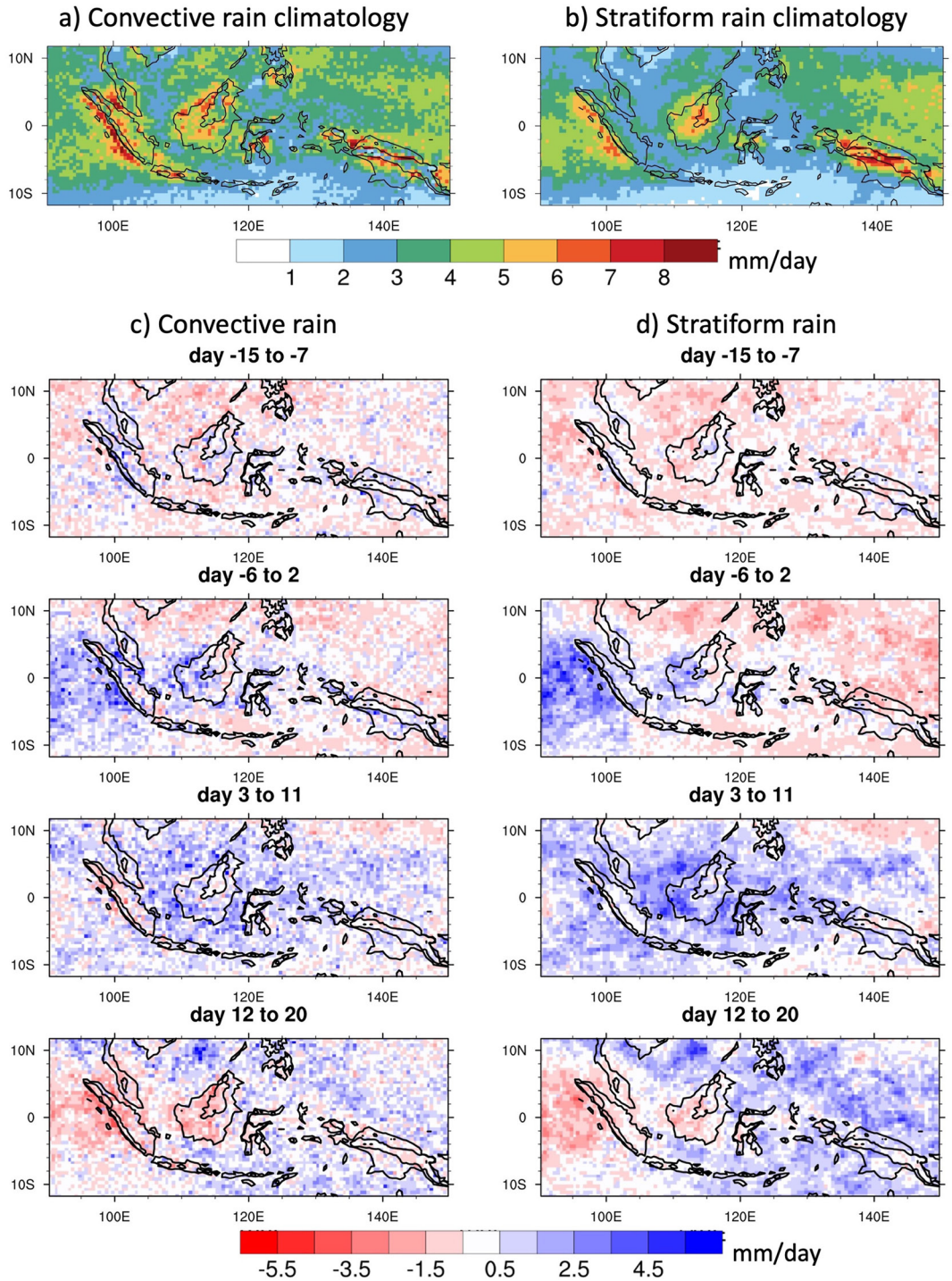

Figure 4. Tropical Rainfall Measuring Mission/Global Precipitation Measurement radar climatology for 2001–2019 of the (a) convective and (b) stratiform precipitation over the Maritime Continent based on 2APR and 2ADPR data. Lag days of unfiltered daily (c) convective and (d) stratiform precipitation, with the Madden-Julian Oscillation at 90°E taken as day 0. Each panel is a 9-day average of the day range indicated in the title. Elevation at 500 m is indicated with black contours.

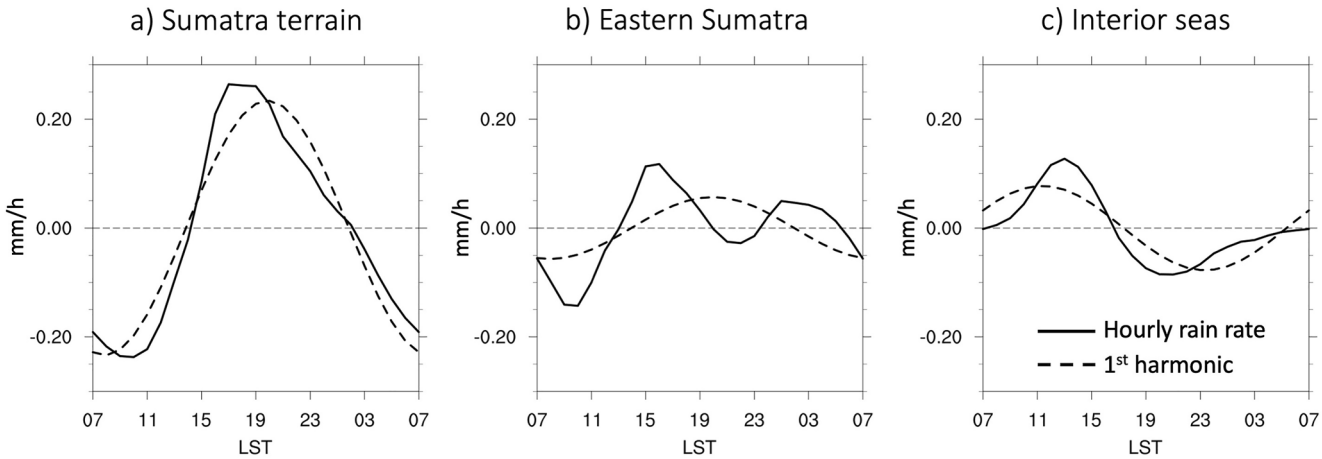

Figure 5. IMERG hourly rain rate (solid) and the corresponding first diurnal harmonic (dashed) for (a) Sumatra terrain, (b) eastern Sumatra and (c) the ocean area between Malaysia and Borneo. Time is in LST.

MJO latent heating leads the deep component over the MC because stratiform rain has a more elevated heating profile than convective rain.

3.2. Diurnal Rainfall Variations

3.2.1. Revisit the Definition of Diurnal Rainfall

Before analyzing diurnal rainfall variations induced by the MJO, we would like to revisit the how diurnal rainfall is defined. One of the most commonly used definitions is to represent the diurnal evolution by the first harmonic of the diurnal Fourier fit, such that the diurnal phase and amplitude can be defined by the phase and amplitude of the first harmonic, respectively (e.g., Birch et al., 2016; Nesbitt & Zipser, 2003; Peatman et al., 2014; Seiki et al., 2021; Yang & Slingo, 2001). However, we argue here that representing tropical diurnal rainfall by the first harmonic may be inappropriate for particular applications.

Figure 5 shows the 19-year averaged diurnal evolution of hourly rain rate from IMERG for three representative regions over both land and ocean around the MC. Over the mountains of West Sumatra (Figure 5a), land convection develops rapidly in the afternoon due to intense surface heating. Convective growth is more of an instantaneous pulse than a sinusoidal oscillation. The first harmonic has a slightly weaker amplitude and a later peak time compared to the maximum hourly rain rate. A similar rapid development of rainfall can also be found over the ocean area between Malaysia and Borneo (Figure 5c), where the maximum near noon is related to the nocturnal offshore rainfall propagation from Borneo (Houze et al., 1981). In this case, the diurnal amplitude is significantly smaller based on the first harmonic and rain peaks earlier. Figure 5b shows the diurnal cycle at the foot of the mountains of eastern Sumatra, where multiple peaks exist. While the afternoon peak is caused by intense land surface heating, the nighttime peak is likely associated with the mountain breeze propagating downslope and eastward at night (e.g., Mori et al., 2004). Besides at the base of mountains, small islands commonly see multiple rainfall peaks due to combined features of land and ocean (Gray & Jacobson, 1977). In these situations, representing the diurnal rainfall by the first harmonic will provide inaccurate information (i.e., a false peak in between multiple peaks) on the diurnal cycle.

Convection develops rapidly in all three cases, no matter when and where the peaks occur, or how many peaks there are. Bai et al. (2021) argued that the oscillating frequency of convection matters to the gravity wave response associated with convective heating. While it is feasible to represent diurnal rainfall characteristics by higher order harmonics, for example, in most cases, the sum of 1–3 diurnal harmonics can represent the diurnal rainfall well, the afternoon convection during its developing phase sometimes contains even higher order harmonics. Therefore, we simplify the definition by using the time of the maximum hourly rain rate as the diurnal rain phase, and the maximum hourly rain rate ($r_{\max}$) minus the daily mean rain rate (r_{daily}) as the diurnal rain amplitude: $r_d = r_{\max} - r_{daily}$.

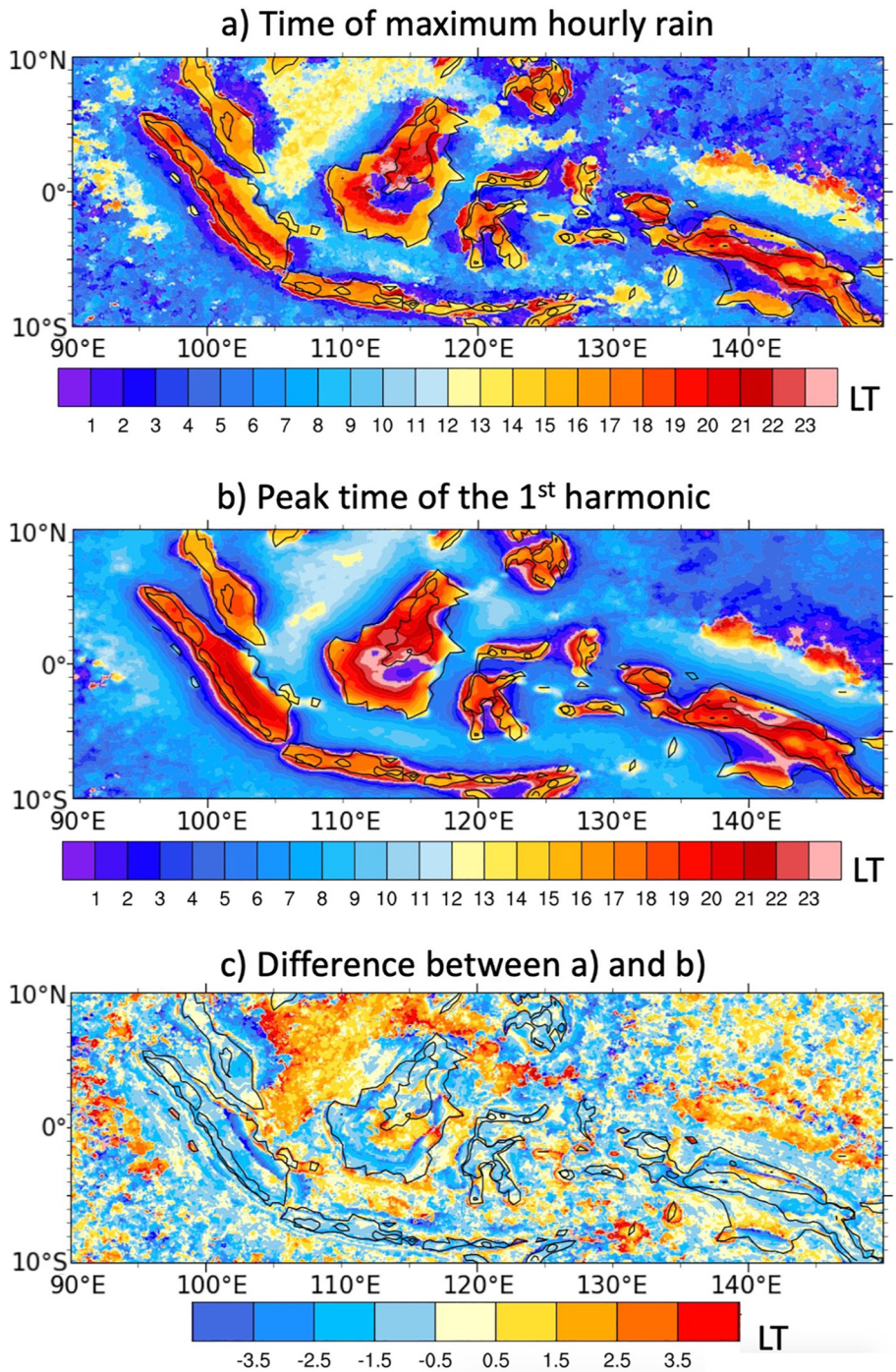

Figure 6. The composite IMERG diurnal phase for 2001–2019 defined by (a) time of maximum hourly rain rate and (b) phase of the first diurnal harmonic. (c) Difference between (a) and (b).

Figure 6 shows geographic variations in the timing of the diurnal peak across the MC using the two diurnal rain definitions described above. Based on the time of the maximum hourly rain rate (Figure 6a), rain peaks from 13 to 20 LT over land (orange to red shading) whereas the phase of the first diurnal harmonic (Figure 6b) generally shows values later in the day (mostly red shading). The difference between the two methods (Figure 6c) indicates a mean lag of 1–2 hr using the first harmonic, consistent with Figure 5a. However, some land regions show even greater differences (e.g., the first harmonic occurs more than 3 hr after the time of maximum rainfall near the east

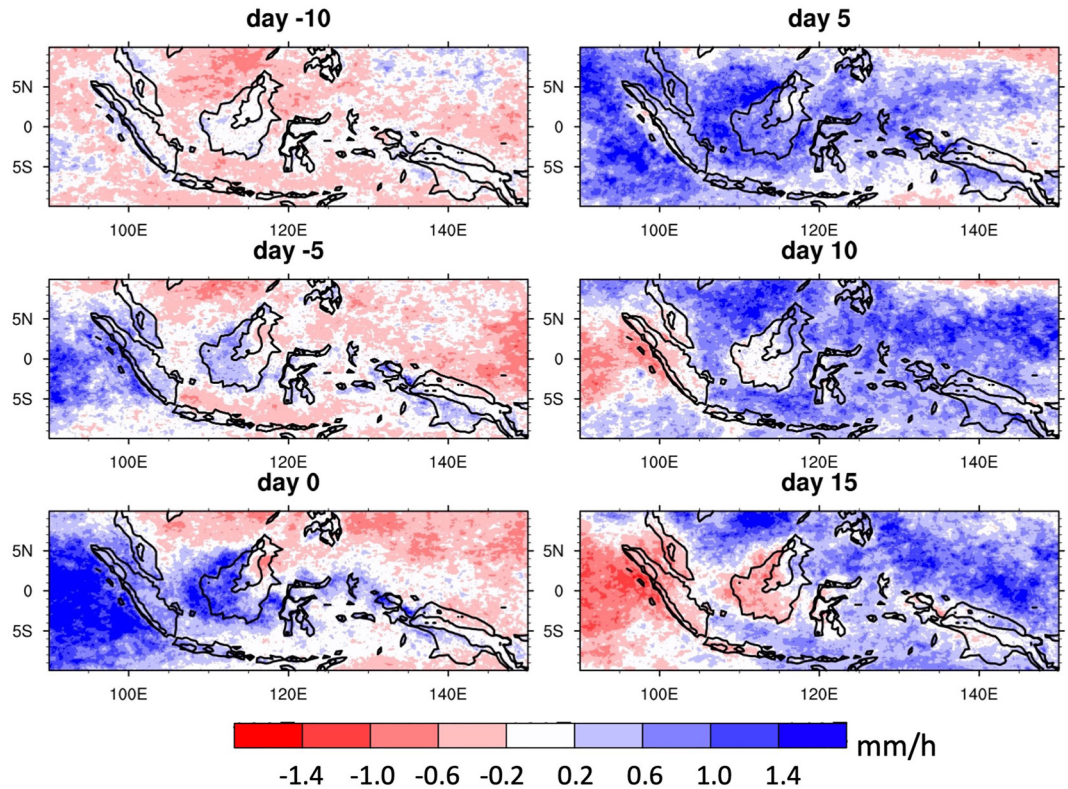

Figure 7. Same as Figure 3, but for IMERG diurnal rainfall amplitude anomalies by Madden-Julian Oscillation lag day.

coast of Sumatra) or regions where the first harmonic peak occurs first (e.g., inland portions of Borneo and New Guinea), likely caused by the smearing of multiple peaks as in Figure 5b.

Over the interior seas, an early afternoon maximum rain rate is observed in Figure 6a (except for the offshore regions from most coasts) while the phase time of the first harmonic is in the late morning in Figure 6b. This causes the mean difference between the two methods to be 1–2 hr (Figure 6c) with the first harmonic peak occurring first, consistent with Figure 5c. Because the diurnal timing differences are in the opposite direction over land and the inland seas, using the time of maximum hourly rain suggests a much stronger diurnal variability than the first harmonic over the MC. As the diurnal timing has implications for assessing things like convective triggering in models, it is important to know the accurate peak time. Different propagation speeds may also be calculated from the different methods, muddying the delineation between gravity waves and land/sea (or mountain/valley) breeze forcing on convective system evolution (Bai et al., 2021). Signals in the diurnal phase are less clear over the open ocean, but also show offsets based on the definition of the diurnal phase used.

We further compared the absolute diurnal rainfall amplitude, defined as the maximum hourly rain rate minus the daily mean rain rate as above, and the normalized diurnal amplitude, which divides the absolute diurnal amplitude by the daily mean $r_d = (r_{\max} - r_{daily})/r_{daily}$ (e.g., Dai et al., 1999). Although the normalized diurnal amplitude is strongly dependent on the daily rain rate, which is influenced by large-scale processes such as the MJO and monsoons, overall changes in the diurnal amplitude with the passage of the MJO are similar for the absolute and relative amplitudes (not shown). Because absolute amplitude shows clearer signals in mountainous and offshore regions during the passage of the MJO, we will use the absolute diurnal amplitude in the rest of the analysis.

3.2.2. Diurnal Rainfall Variations

Figure 7 shows lag days of the diurnal rainfall amplitude anomalies for the 89 MJO events compared to climatology, with the MJO at 90°E taken as day 0. The pattern of the anomalous diurnal rainfall amplitude resembles the anomalous daily rainfall in Figure 3 and shows the asymmetry to the west and east of the MC orography with the MJO. Lu et al. (2019) also reported that the diurnal rainfall maximizes during phases 2–3 (i.e., prior to the

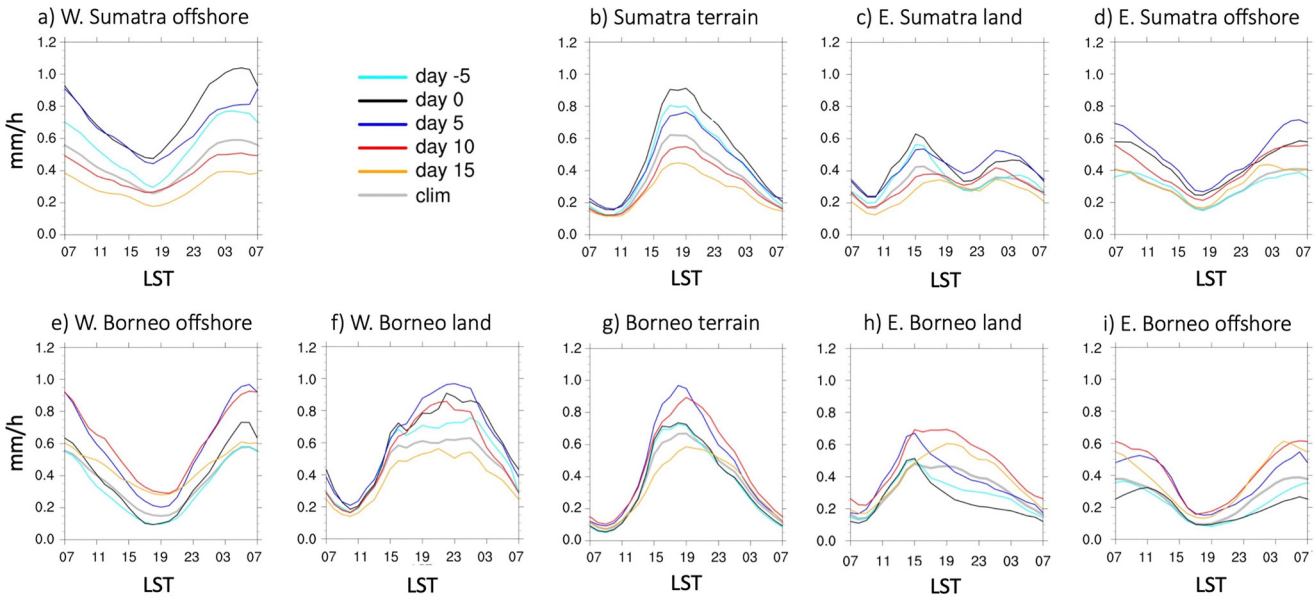

Figure 8. Hourly rain rate on the Madden-Julian Oscillation lag days to the west of (left two columns), over (mid column), and to the east of (right two columns) the mountains on Sumatra (upper row) and Borneo (lower row). Panels (a–i) correspond to regions denoted by black boxes in Figure 1 with letters A-I, respectively. Lag day definition is the same as Figure 7. Time is in LST.

active MJO) using TRMM 3B42, but did not address the east-west contrast. The similar patterns of changes in the daily and diurnal rainfall indicate that when the daily mean increases, the peak of the diurnal rainfall is also enhanced with the passage of the MJO, which will be further elucidated in Figure 8. While Peatman et al. (2014) did not find a clear relationship between the diurnal rainfall anomalies and topography using the 3-hourly TRMM 3B42 product at its innate 0.25° resolution, Sakaeda et al. (2020) reported that the diurnal rainfall on the east side of orography lags the west side as the MJO passes, with the diurnal rainfall determined using the first harmonic of the 3-hourly TRMM 3B42 product gridded to 0.5° resolution. Using the Climate Prediction Center morphing technique (CMORPH) precipitation and defining the diurnal rainfall with the first harmonic, Natoli and Maloney (2019) further found contrasting diurnal rainfall characteristics on the two sides of Luzon Island in the Philippines during the boreal summer intraseasonal oscillation. The location- and MJO phase-dependent diurnal rainfall was also demonstrated by Qian (2020) and Da Silva and Matthews (2021) using CMORPH and IMERG precipitation, respectively. Our results show that the contrasting features on the two sides of the MC islands with the propagation of the MJO is robust using different diurnal definitions and datasets.

Nevertheless, the use of a higher resolution data set (i.e., hourly and 0.1°) and defining the diurnal cycle by the hour of maximum rainfall instead of the first harmonic allows us to look into more detailed changes of the MJO-induced diurnal rainfall associated with topography. Figure 8 shows hourly IMERG rainfall on different lag days to the west of, over, and to the east of the mountains on Sumatra and Borneo. The regions are delineated on the map in Figure 1. New Guinea is not shown because it has similar MJO-induced diurnal rainfall changes as Sumatra due to an analogous long and narrow mountain configuration.

Rainfall over the mountains on Sumatra and Borneo peaks between 16 and 19 LT (Figures 8b and 8g), consistent with the peak time over high terrain in the US (Carbone & Tuttle, 2008). Borneo shows more variability in the timing of peak rainfall by MJO phase, with a shift from 16 to 19 LT as the MJO approaches the island, possibly due to enhanced cloud cover delaying the onset of convection. The diurnal rainfall over the orography reaches its maximum on days 0 and 5 on Sumatra and Borneo, respectively, corresponding to the dates when the active MJO reaches the longitudes of the islands. In addition, the diurnal rainfall amplitude begins to increase before the peak date on the islands, in agreement with Figure 7. This is because prior to the active MJO, clear skies over the MC assist daytime land heating and convective development, and afternoon rainfall is enhanced (Hagos et al., 2016; Peatman et al., 2014).

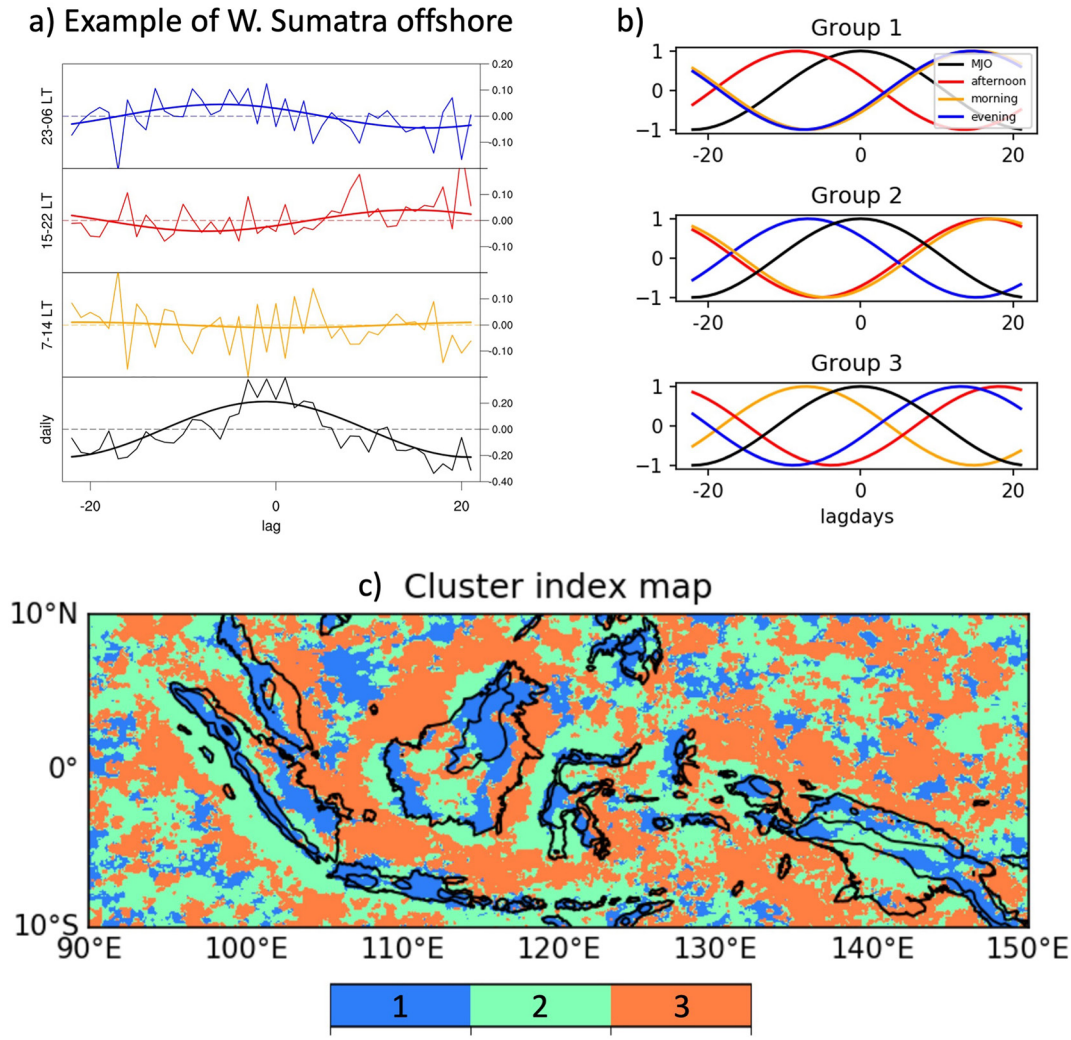

Figure 9. (a) An example time series from offshore of western Sumatra of the diurnal Madden-Julian Oscillation (MJO) rainfall anomalies averaged for 7–14 LT (morning), 15–22 LT (afternoon) and 23-06 LT (nighttime) with the passage of the MJO. The bottom panel is the daily rainfall anomaly by MJO lag day. (b) The three cluster groups from the K-means clustering over the Maritime Continent. (c) Map of the cluster index corresponding to (b).

Similar to Sumatra terrain, the total rainfall within a few hundred km offshore from West Sumatra (Figure 8a) increases prior to the active MJO and decreases afterward. While a single peak is observed on all lag days, the peak time shifts from 3 LT on day −5 to 5 LT on day 0, suggesting a slower offshore rainfall propagation likely due to the changing large-scale winds associated with the passage of the MJO (Bai et al., 2021). The offshore region east of Sumatra (Figure 8d) also shows a single early morning peak and the total rainfall maximizes on day 5, lagging the western offshore region. A similar comparison can be made for the western and eastern offshore regions of Borneo (Figures 8e and 8i), which have a single early morning peak around 5 LT with the diurnal rainfall to the west peaking on days 5–10 (similar to Borneo terrain, albeit a few hours after the West Sumatra offshore peak), while offshore rainfall to the east of Borneo peaks on days 10–15, lagging the west.

Over the land region just west of the Borneo topography (Figure 8f; an analogous region over West Sumatra doesn't exist because the mountains are adjacent to the western coast), the total rainfall increases before the MJO arrives, reaching maximum amounts on days 0–5, and decreases afterward. The evening peak occurs before midnight but after the peak rain over the terrain, presumably due to interactions between the sea breeze and mountain flows, and is most pronounced on days −5–5. The rainfall distribution broadens on days 10–15 and the peak time becomes earlier, indicating reduced nocturnal rainfall forcing.

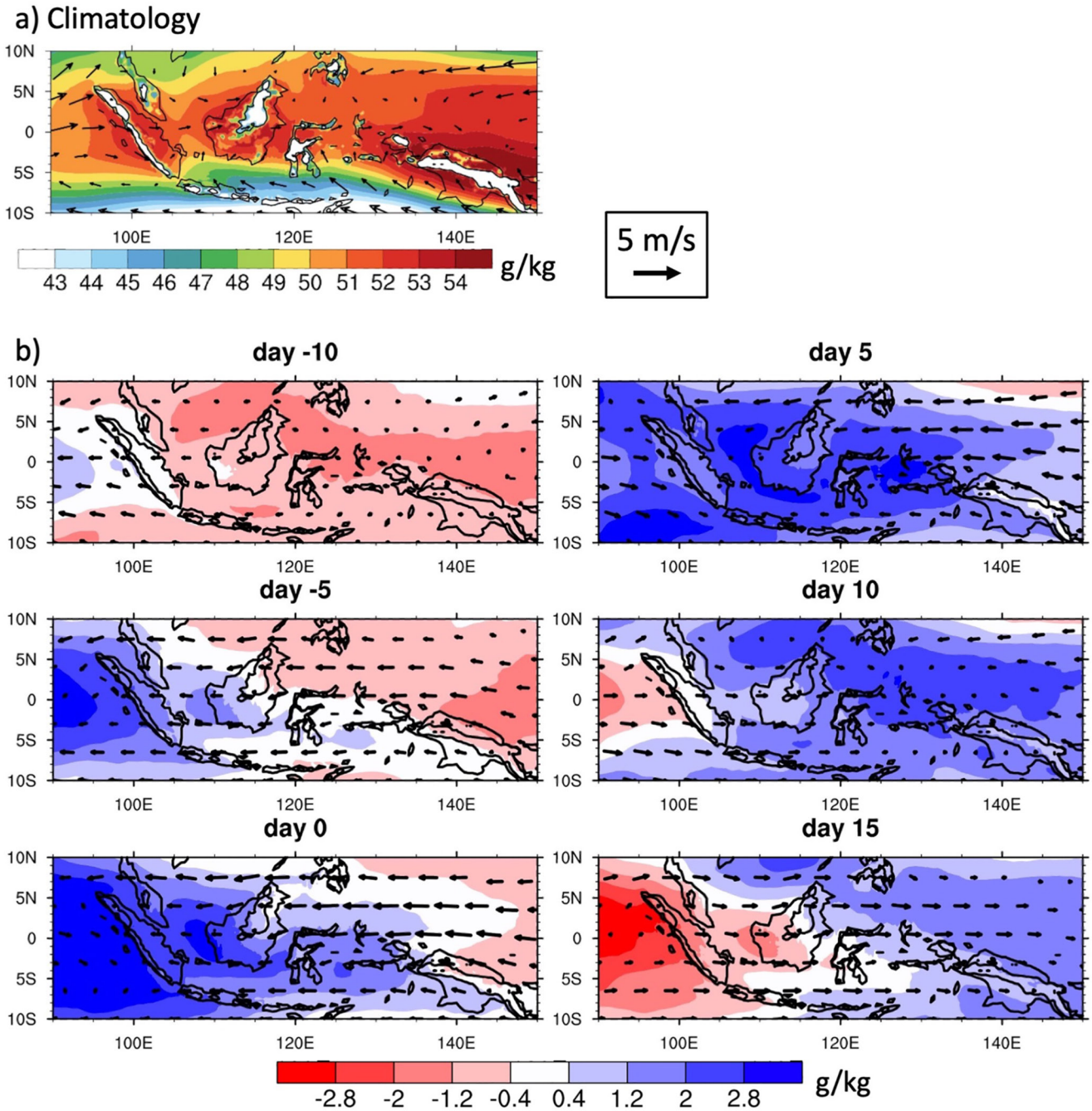

Figure 10. (a) Climatology of the ERA5 column specific humidity and 850-hPa winds for 2001–2019. (b) Same as Figure 3, but for the ERA5 intraseasonal column specific humidity overlaid by intraseasonal 850-hPa winds.

For the land region to the east of the Sumatra topography (Figure 8c), two diurnal rain peaks are observed, one in the afternoon around 15 LT, another at night around 2 LT. The afternoon land convection peak is caused by strong surface heating, but its earlier peak time than over the mountains is likely associated with the daytime sea breeze circulation (Burpee & Lahiffi, 1984). The nighttime peak is presumably related to the nocturnal mountain breeze causing downslope rainfall propagation (Houze, 2012; Kousky, 1980; Mapes et al., 2003). However, the relative importance of each of these forcings varies by island and by MJO phase. For example, the afternoon and nighttime peaks are of equal magnitude over eastern Sumatra, but the afternoon peak is consistently larger over eastern New Guinea (not shown). Over eastern Borneo (Figure 8h), the afternoon peak dominates as the MJO

approaches due to clear sky conditions, while a broader evening peak dominates as the MJO recedes (opposite of what happens to the west of the Borneo topography). A similar lag between the afternoon and nighttime peaks can also be observed over eastern Sumatra between days 0 and 5 and the afternoon peak becomes later while the nighttime peak occurs earlier as the MJO passes over Sumatra. In summary, several factors can contribute to the diurnal rainfall variations over the mountainous islands of the MC as the MJO passes: surface heating by solar radiation, the moisture supply, synoptic winds, and locally forced low-level winds. An analysis of the impacts of moisture and winds on diurnal rainfall be given in Section 4.

To better highlight the distribution of the location-dependent diurnal rainfall changes at each grid point with the passage of the MJO, the K-means clustering method was used. We first calculated diurnal rainfall anomalies by subtracting the daily mean rain rate from the hourly rain rate to remove the MJO-induced daily rainfall. The hourly rain rate anomaly was then averaged into three clumps: 7–14 LT, 15–22 LT, and 23-6 LT, corresponding to morning, afternoon/evening, and nighttime rain, respectively. Results are not sensitive to slightly different definitions of the clumps (e.g., 6–13 LT as morning rain instead of 7–14 LT). The three clumps of diurnal rain anomalies at each grid point were Fourier fitted with the MJO harmonic as well as the daily rainfall used in Figure 3. Using the offshore region west of Sumatra as an example, Figure 9a shows the time series of the three clumps of diurnal rainfall anomalies with the passage of the MJO, along with the associated daily rainfall anomalies for reference. According to the method used to define the clumps, the three lines for the original diurnal rainfall sum up to zero and it is the same for the three Fourier fit lines. Thus, changes in the amplitude of the three clumps are not the absolute value, but the relative changes compared among the three clumps. Figure 9a shows that the nighttime rain peaks before the main body of the MJO offshore of West Sumatra, the morning rain has a weaker MJO harmonic (note the different *y*-axis scales), and the afternoon rain is slightly reduced before the MJO because the three diurnal rainfall clumps sum up to 0.

The K-means clustering method was then applied based on the phases of the three diurnal rainfall time series at each grid point relative to the MJO phase. The optimal K was determined to be three using the Elbow curve (Thorndike, 1953) of the explained variation. The K-means clustering was also applied using the diurnal amplitude but the result turned out to be insensitive to the amplitude, perhaps because the amplitude of one diurnal clump is constrained by the other two due to the zero-sum limitation. Therefore, only the diurnal phase of the three clumps was used to cluster features. Different initiations were used to find the best output in terms of inertia. Figure 9b shows the resulting three cluster groups. Afternoon, nighttime, and morning rain peaks before the MJO main body in the three cluster groups, with the other two clumps peaking after the MJO daily rain.

Figure 9c is the map of the corresponding cluster index. Areas over the mountains on the MC islands are clustered into the first group, where the afternoon rain peaks before the MJO daily rain. As mentioned before, this is because clear skies over the MC prior the MJO are favorable for land convective development. Regions west of the mountains (up to 300 km or so) are clustered into the second group, where the nighttime peak is ahead of the MJO regardless of whether the region is offshore or over land because of low-level convergence between the land/mountain breeze and prevailing synoptic westerlies. Land regions east of mountains tend to be categorized into a mix of the first and the second groups, which is due to shifting of the dominant rainfall from the afternoon to nighttime (Figures 8c and 8h), indicating variations in insolation and low-level winds are of comparable importance. Because the diurnal rainfall in offshore regions east of the mountains lags the offshore regions west of the mountains, east offshore regions are clustered into the third group, where the afternoon and nighttime offshore rainfall peaks after the MJO. The distribution of different diurnal rainfall changes near the islands is consistent with the changes shown in Figure 8. Signals over the open ocean farther away from the islands are noisier, indicating that the diurnal rainfall changes described above are closely tied to topography/land. Therefore, the diurnal rainfall changes are strongly dependent on location to the west of, over, and to the east of the MC mountains when the MJO passes.

4. MJO Moisture and Wind Patterns

4.1. Atmospheric Moisture Budget

The goal of this section is to quantify what determines the contrasting features of the MJO-induced daily and diurnal rainfall to the west and east of the MC orography. The diurnal rainfall anomalies in Figure 7 closely follow the daily rainfall anomalies in Figure 3, indicating that the anomalous diurnal rainfall is synchronized

with the anomalous daily rainfall with the MJO. The synchronization can also be seen in Figure 8, where the primary diurnal peak is enhanced as the daily rainfall increases with the MJO, consistent with Tian et al. (2006). Therefore, explaining what determines the east-west asymmetry related to topography in daily rainfall will also explain what determines the diurnal rainfall asymmetry. Figure 10a shows the mean vertically integrated surface to 300 hPa (hereafter, column) specific humidity and 850-hPa winds from ERA5 for 2001–2019. The highest amounts of moisture are found over the MC islands (except for high-elevation orography) and the West Pacific warm pool. Near the equator, westerlies and easterlies converge near 120–130°E. To identify the MJO-induced anomalous wind and moisture, daily wind and specific humidity were separated into low-frequency (>100 days), intraseasonal (20–100 days), and high-frequency (<20 days) time scales following Jiang et al. (2019). Figure 10b shows lag days of intraseasonal column specific humidity, overlaid by intraseasonal 850-hPa winds. High moisture air associated with the MJO moves eastward over the MC, followed by drier air around day 10. Anomalous easterlies exist to the east of the propagating high-moisture anomaly and anomalous westerlies exist to the west, consistent with Zhang (2005) and Adames and Kim (2016). Variations in moisture during the MJO are roughly 15% of the climatological mean over the ocean and less than 10% over land, while MJO variations in low-level winds are comparable to the mean winds.

Based on the moisture budget in an atmospheric column, precipitation (P) can be represented as:

$$P = -\frac{\partial}{\partial t}\frac{1}{g\rho_w}\int_0^{p_s} q\,dp + \frac{1}{g\rho_w}\int_0^{p_s} -\nabla\cdot(q\mathbf{V})\,dp + E \tag{1}$$

where g is gravitational acceleration, ρ_w is liquid water density, q is specific humidity, $\mathbf{V}$ is horizontal wind, p_s is surface pressure, and E is evaporation. The first term on the right hand side is the column moisture storage, and the second term is column-integrated moisture flux convergence (MFC). Other forms of atmospheric liquid and frozen water are ignored.

MFC can be used as a diagnostic measure for convective development. Based on observations made during the Dynamics of the Madden–Julian Oscillation (DYNAMO) Indian Ocean field campaign, Johnson and Ciesielski (2013) and de Szoeke et al. (2015) reported that MFC is the dominant moisture source for the intraseasonal and daily precipitation anomalies. MFC is defined as: $MFC = -\mathbf{V}\cdot\nabla q - q\nabla\cdot\mathbf{V}$, where $\mathbf{V} = \vec{u} + \vec{v}$. The terms on the right hand side correspond to moisture advection and moisture convergence, respectively. The filtered variables u, v, and q at high-frequency, intraseasonal and low-frequency time scales will be denoted with subscripts h, i and l, respectively. Due to the MJO event selection, averaging, and filtering described in previous sections, changes in the low-frequency variables are negligible when plotted as lag days of the passage of the MJO (not shown). Therefore, the low-frequency variables will be taken as equivalent to the climatology in this study.

Figures 11a shows the MJO lag days of column MFC anomalies with the low-frequency column MFC ($-\mathbf{V}_l\cdot\nabla q_l - q_l\nabla\cdot\mathbf{V}_l$) removed. This anomalous MFC pattern largely captures the detailed features of the anomalous daily rainfall over the island topography in Figure 3 as the MJO passes. Quantitatively, the anomalous MFC in Figures 11a supplies roughly 65% of the moisture to the daily precipitation anomalies in Figure 3. The dominant contribution from MFC is consistent with the previously mentioned studies. The total MFC can be further decomposed into moisture convergence and moisture advection of the low-frequency, intraseasonal, and high-frequency moisture by the low-frequency, intraseasonal, and high-frequency wind, resulting in a total of 18 terms. With the low-frequency MFC taken out in Figures 11a, the rest 16 of the terms were investigated to find the determining processes for the rainfall amplitude anomalies.

The largest term contributing to the anomalous column MFC is moisture convergence of the low-frequency moisture by the MJO anomalous winds (Figures 11b, note that the column MFC is calculated using moisture and winds at all surface-to-300 hPa levels, but only 850-hPa winds are shown here), which accounts for over 80% of the variation of MFC anomalies in Figures 11a. The second most important term contributing to the east-west precipitation contrast is moisture advection of the low-frequency moisture by the MJO anomalous winds (Figures 11c), which is an order of magnitude smaller than the moisture convergence term. While moisture convergence has large impacts over both land and ocean, moisture advection is closely tied to the islands and indicates a clear contrast between the west and east side of the topography as the MJO passes, with a reverse in sign after day 5. To better quantify contribution of moisture convergence and advection to the east-west asymmetry in rainfall anomalies relative to topography/land, we further calculated the variance explained by moisture convergence and advection over land and its nearby oceans only (i.e., oceanic regions less than 500 km away

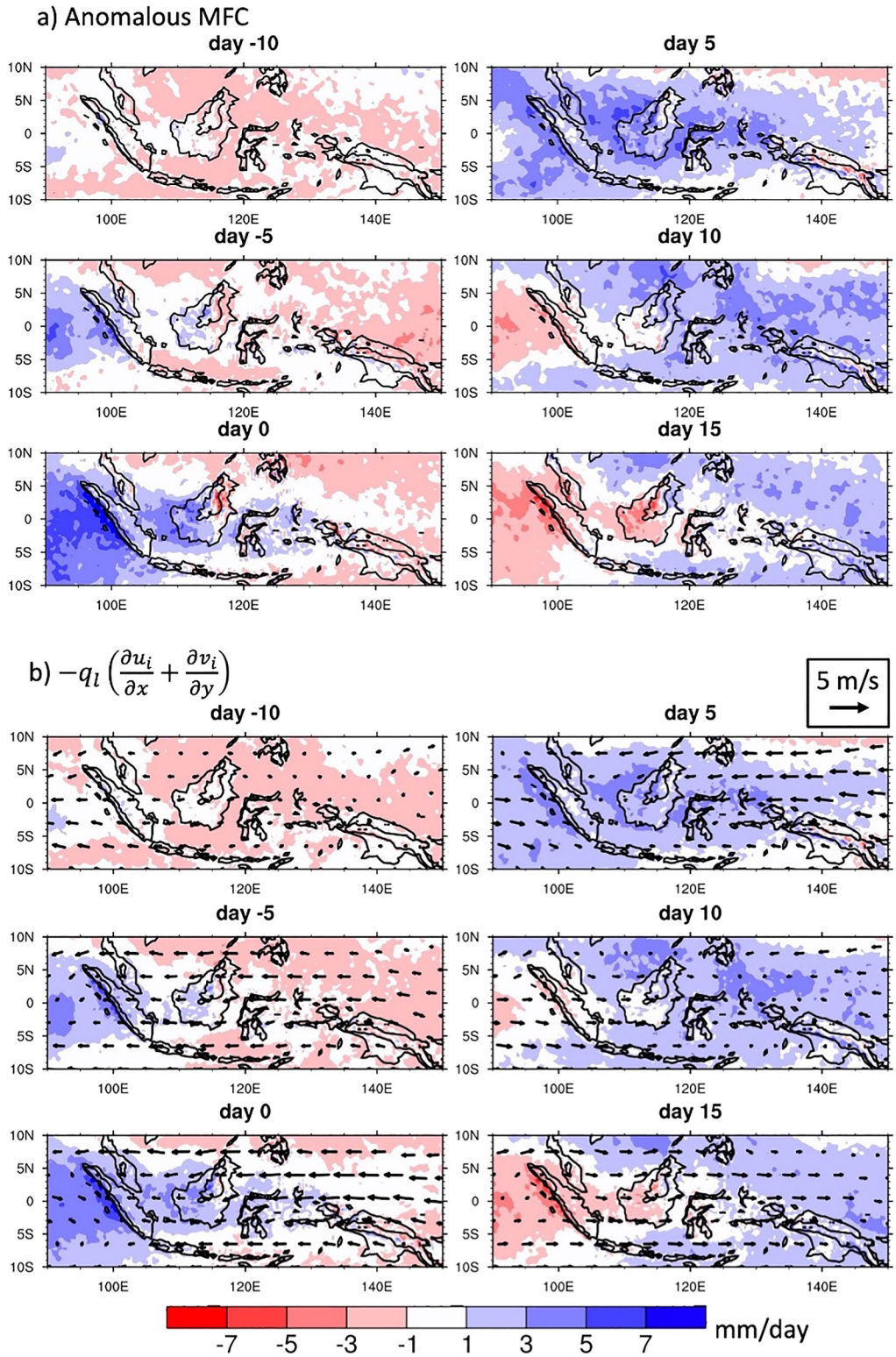

Figure 11. Same as Figure 3, but for the ERA5 (a) column moisture flux convergence (MFC) anomalies compared to the low-frequency MFC, (b) column moisture convergence of low-frequency moisture by intraseasonal wind, (c) column moisture advection of low-frequency moisture by intraseasonal wind, and (d) column moisture convergence of low-frequency moisture by high-frequency wind. For reference, intraseasonal and high-frequency 850-hPa wind anomalies are overlaid on (b–d), respectively. The same color bar from Figure 3 is used for (a and b) for comparison, while the color bar for (c and d) represents a smaller range.

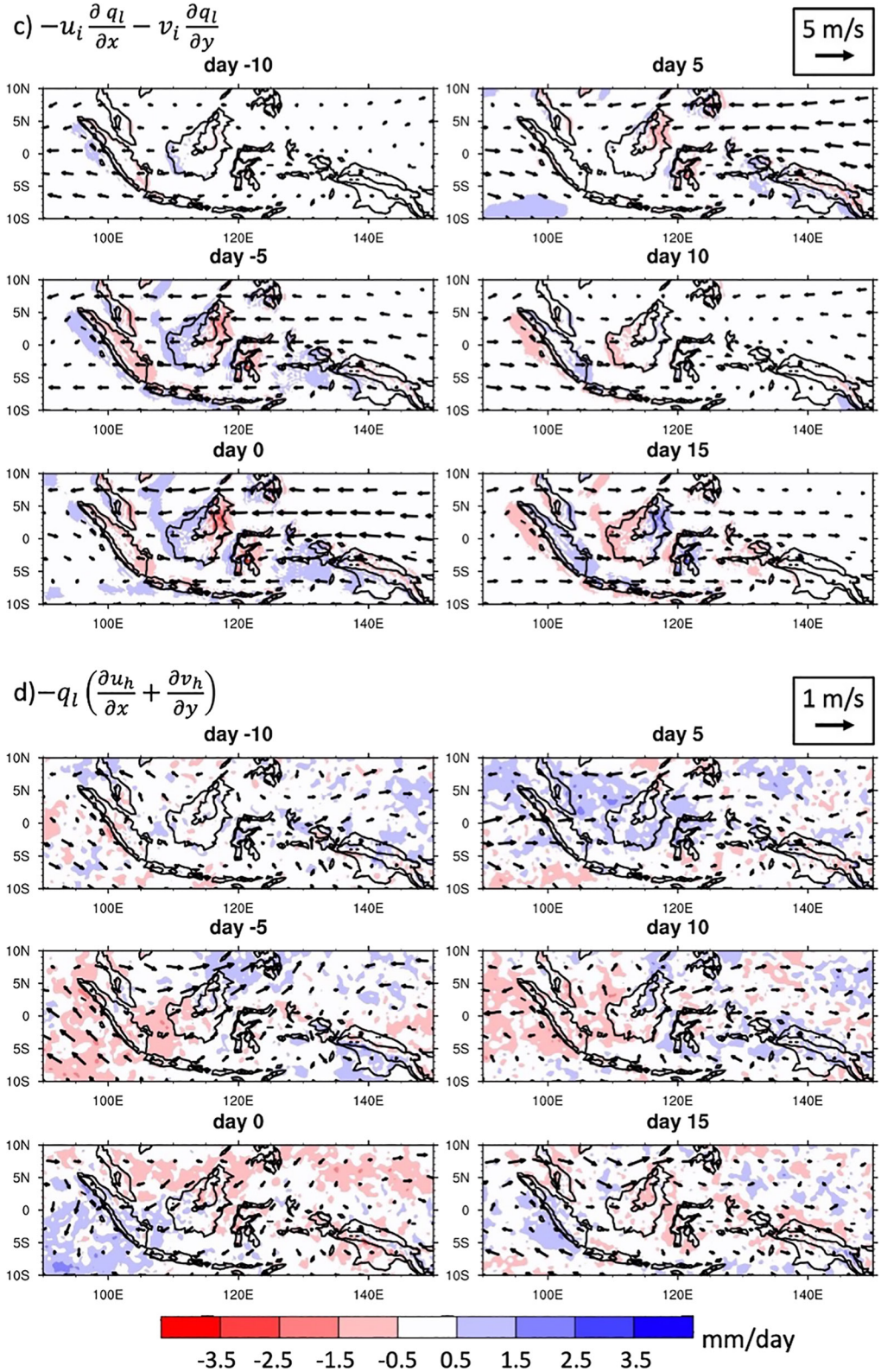

Figure 11. (Continued)

from land). Results show that moisture convergence explains 79% of the MFC anomalies and moisture advection explains about 9%. In Figures 11b and 11c, the horizontal MJO wind is intercepted by the topography, leading to a discontinuous wind gradient on both sides of the mountains (not shown). For example, when easterlies are present, the wind gradient will be positive to the west of the orography and negative to the east, generating asymmetry in divergence relative to the MC mountains (i.e., divergence to the west and convergence to the east), which further leads to asymmetry in MJO vertical velocity on either side of the mountains. A special term that also arises is moisture convergence of the low-frequency moisture by high-frequency winds (Figures 11d). While lagged moisture convergence can be observed on the two sides of the topography, its frequency is higher and on an order of roughly 15 days, which may be related to other higher frequency equatorial waves. However, this term is not coherent with the anomalous rainfall amplitude and therefore not a main contributor. The rest of the terms are generally negligible compared to the three terms above. While Lu et al. (2019) reported that convergence by diurnal wind is important to determine the diurnal rainfall anomalies over the MC during the MJO, their analysis of divergence associated with diurnal wind did not show an east-west asymmetry around the topography. Comparing with our analysis above, we demonstrate that the east-west rainfall asymmetry (daily and diurnal) may not be associated with diurnal-scale variations in moisture or wind, but longer-scale variations.

The magnitude of the MFC terms can be understood using Figure 10, where variations in intraseasonal moisture are small compared to the climatological mean while variations in the intraseasonal low-level winds are comparable to the mean winds. Sakaeda et al. (2020) reported that low-level wind patterns are important to the diurnal rainfall, but they did not find a significant correlation between the column-integrated specific humidity and the diurnal rainfall peak either over land or ocean during the MJO. According to our results, this may be due to the small variations of the anomalous MJO moisture making it a secondary contribution to the anomalous MFC. Our results highlight the dominant role of both the MJO anomalous winds and the mean moisture in determining the anomalous diurnal rainfall amplitude. The diurnal rainfall asymmetry over the MC islands may also be impacted by the monsoonal flow and therefore have seasonal variability (Qian, 2020).

4.2. Impact of Wind on Diurnal Rainfall Over Islands With Topography

Land rainfall can propagate toward and away both sides of an island. Afternoon land convection can propagate up to many hundreds of kilometers offshore in the evening to early morning and can also propagate inland, but earlier than offshore rainfall (e.g., Biasutti et al., 2012; Kikuchi & Wang, 2008; Mori et al., 2004; Yang & Slingo, 2001). The timing and speed of the rainfall propagation is closely related to land-sea and mountain-valley breezes that are present, as well as background winds. Rain systems will propagate faster and reach farther distances when the large-scale, low-level wind is in the same direction of the rainfall migration, whereas rainfall will be slowed down or even prevented from propagating if the low-level wind is in the opposite direction of the rainfall migration (e.g., Du & Rotunno, 2018; Ichikawa & Yasunari, 2007; Mori et al., 2004; Qian, 2020; Sakurai et al., 2005; Short et al., 2019; Wang & Sobel, 2017; Yokoi et al., 2019). To better understand the role of the MJO-induced winds on diurnal rainfall variations at different locations in the MC, the Pearson correlation coefficient was calculated to quantify the relationship of the diurnal rainfall anomalies (regridded from 0.1° to 0.25° to match the ERA5 resolution) with low-level winds.

Figure 12 shows the linear cross correlation map at a lag of 0 between the diurnal rainfall amplitude and the 850-hPa winds at each grid point perpendicular to the coasts of Sumatra, Borneo and New Guinea. Up to about 150 km offshore from West Sumatra, diurnal rainfall decreases with an increased MJO-induced wind component toward the island. However, this negative correlation is only statistically significant from about 3°N to 2°S. Using C-band radar data from Padang (located near the equator on the west coast of Sumatra), Bai et al. (2021) demonstrated that strong westerly low-level winds prevent land convection from propagating offshore from Sumatra during the active MJO. These findings suggest that MJO wind modulation of offshore rainfall evolution is valid when close to topography/land, while the relationship is insignificant over the open ocean. Over eastern Sumatra, the nighttime peak occurs earlier and the afternoon peak occurs later as the MJO passes by (Figure 8c), indicating a faster rainfall propagation at night and weaker sea breeze during the day with stronger westerlies, respectively. However, Figure 12 shows a negative correlation between the diurnal rainfall amplitude and the westerlies, suggesting that stronger southwesterly winds contribute to the reduction of the diurnal rainfall peak. The reduction in the peak amount in East Sumatra, as opposed to other islands, may be related to the change in peak time

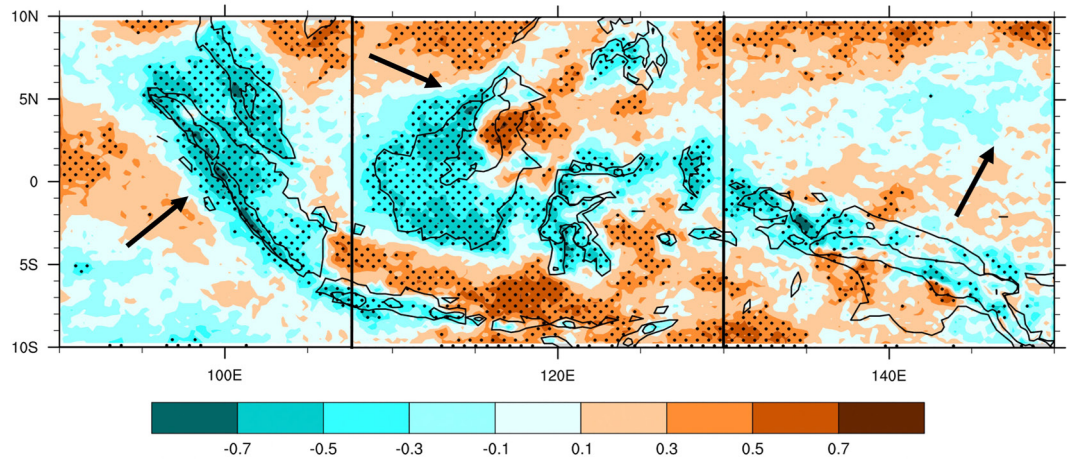

Figure 12. Map of pointwise linear cross correlation coefficients at a lag of 0 between time series of the diurnal rainfall amplitude for the 89 Madden-Julian Oscillation events with 850-hPa winds that are perpendicular to Sumatra (90–107°E), Borneo (107–130°E) and New Guinea (130–150°E), respectively. Wind directions perpendicular to the islands are indicated with black arrows. Stippled areas are statistically significant at $\alpha = 0.05$ based on a student *t*-test.

demonstrated in Figure 8c. In contrast, the offshore region of East Sumatra shows a weak positive correlation, indicating that stronger westerlies help with the offshore rainfall propagation to the east.

In west Borneo (center panel of Figure 12), the diurnal rainfall decreases with an increased westerly component. As westerlies associated with the MJO gradually increase, the maximum diurnal rainfall changes from night on days −5 to 5 to the late afternoon on day 10 as the MJO passes (Figure 8f), because stronger westerlies can slow down or even prevent rainfall from propagating to the west. In contrast, the diurnal rainfall increases with increased westerlies over eastern Borneo where moisture does not show a significant correlation with the diurnal rainfall, suggesting that the low-level zonal wind may be the primary determining factor. Before the MJO reaches Borneo, strong easterlies to the east Borneo prevent nocturnal downslope rainfall from moving eastward and the nighttime peak is reduced (days −5 to 0; Figure 8h). As the MJO passes Borneo with an increased westerly component, the nighttime rainfall increases gradually from days 5–15. Although the reduced nighttime rainfall accompanied by the enhanced afternoon rainfall as the MJO passes can also be observed over western New Guinea from days 5 to day 10 (not shown), Figure 12 (right panel) does not indicate a significant correlation between the diurnal rainfall and wind perpendicular to the topography, and moisture seems to play a bigger role. This may be because the MJO weakens over the MC, and its lessened influence on New Guinea can also be inferred from the smaller deviation from the diurnal rainfall climatology (not shown). Therefore, the relationship between the diurnal rainfall and MJO winds is location dependent and its relative importance also varies island to island, especially when considering wind components perpendicular to topography.

Although higher wind speeds can help rainfall propagate faster and farther in the same direction, Wang and Sobel (2017) showed that island-averaged rain reaches a minimum when the background low-level wind speed is roughly 5 m/s, indicating a nonlinear relationship between island rain amount and low-level wind. Thus, both the geographical rainfall distribution and amount are functions of wind speed. However, it is difficult to isolate the influence of the MJO winds from other MJO-induced large-scale environmental changes using observations alone, and modeling work is needed to quantify wind modulation under the influence of the MJO. Furthermore, the island rainfall-wind relationship found by Wang and Sobel (2017) applies to terrain up to 800 m. To what extent the relationship will be altered to by the high MC terrain remains unclear.

Moreover, vertical shear of the horizontal wind may also play a role in modulating different types of rain. Bai et al. (2021) showed that the speed of the stratiform rain propagating to the west is faster than convective rain in the offshore region west of Sumatra due to a westward upper-level wind shear. Using WRF, Du et al. (2019) reported that wind speed shear can change the shape of the land–sea breeze circulation/gravity waves, thus modulating the rainfall propagation. Mid-level wind increases as the MJO passes the islands, leading to a larger wind shear at both lower and upper levels (not shown). Although beyond the scope of this study, open questions

concerning the wind shear modulation of rainfall include: How will the rainfall-wind relationship change if the horizontal wind is sheared instead of vertically uniform? Will the wind shear change organization of the diurnal land convection? What is the relative importance of the change in the wind shear compared to change in the mean wind to the diurnal rainfall distribution?

5. Summary and Conclusions

This study investigates impacts of the MJO on the daily and diurnal rainfall over the MC, with a particular focus on influences of island topography. Comparing with previous studies using the first diurnal harmonic, the diurnal rainfall in this study is defined using the maximum hourly rain rate because the diurnal cycle contains higher frequency components and the first harmonic may miss details and even produce false peaks. Defining the diurnal rainfall by maximum rain rate also gives different timing than the first harmonic across the MC. In general, the phase of the maximum hourly rain is 1–2 hr earlier than the first harmonic in places where afternoon and evening rain dominates (e.g., much of the islands and coastal ocean), while the phase of the maximum hourly rain is 1–2 hr later than the first harmonic where there is morning rain (e.g., the inner and open oceans, central Borneo, and parts of western New Guinea).

A total of 89 MJO events encountering the MC were identified during 2001–2019 using TRMM/GPM IMERG data. Based on lag day analysis of the 89 MJOs, contrasting features are found to the west and east of the topography of three major MC islands: Sumatra, Borneo and New Guinea. The daily rainfall on the west side of the topography peaks a week earlier than the surrounding ocean, whereas the east side is roughly in phase with the surrounding ocean. Such a lag between the west and east of the topography can also be found in the anomalous diurnal rainfall amplitude. In addition, the east side of the mountains experiences smaller daily rainfall variations compared to the west, in part because of smaller annual mean precipitation to the east. We found that the rainfall on either side of the topography has similar convective and stratiform rain contributions when the MJO is active over the MC.

A single, sharp daytime peak is found over the topography of the three major islands around 19 LT; however, two peaks are observed east of the topography over land, one in the afternoon (15 LT) associated with surface heating and the sea breeze and another at night (around 2 LT) caused by downslope winds from the mountains. The diurnal maximum over land to the west of topography has a broad evening peak and an early morning peak is found over the offshore oceans. To the west of the topography, regardless if it is land or offshore ocean, the nighttime peak increases before the MJO arrives then gradually decreases as the MJO passes over. In the meantime, the peak time gets earlier. In contrast, to the east of the topography, the afternoon peak is enhanced prior to the MJO while the nighttime peak is enhanced after the MJO. The K-means clustering method better shows that the diurnal rainfall changes are strongly dependent on location to the west of, over, or to the east of the mountains when the MJO passes. Signals over the open ocean farther away from the islands do not show such a dependence, suggesting that the MJO-induced diurnal rainfall features closely follow topography/land.

The schematic in Figure 13 summarizes findings of Figures 3, 4, and 7–9 and the location-dependent MC diurnal rainfall changes as the MJO passes. In offshore regions to the west of the orography, reduced westerlies prior to the MJO allow faster nocturnal offshore rainfall propagation associated with the land breeze, while the enhanced westerlies during the active MJO slow down the land breeze convergence, leading to later nighttime peaks. The western offshore regions are in cluster 2, where the nighttime rainfall increases before the MJO arrives. An opposite relationship between nighttime rainfall and MJO westerlies can be drawn for the eastern offshore regions, where the nighttime rainfall shifts earlier and increases in magnitude after the active MJO (cluster 3). Prior to the active MJO, clear sky conditions with more insolation enhance the afternoon convection over land, no matter to the west, over, or to the east of the mountains. The single late afternoon peak over the terrain is thereby in cluster 1, where the late afternoon rainfall is enhanced before the MJO. Over low-elevation land to the west of orography, reduced westerlies before the MJO allow faster and enhanced nocturnal rainfall propagation associated with the mountain breeze. While the afternoon rainfall is also enhanced due to clear skies before the MJO, changes in the nighttime rainfall dominate the diurnal variations (e.g., Figure 8f), so low-elevation land to the west is grouped into cluster 2. However, no single cluster can summarize diurnal rainfall changes over land to the east of the orography (Figure 9c). The mixed clustering is caused by the dominant rainfall shifting from afternoon to nighttime (Figures 8c and 8h), with impacts of variations in insolation and low-level winds being comparable. In addition,

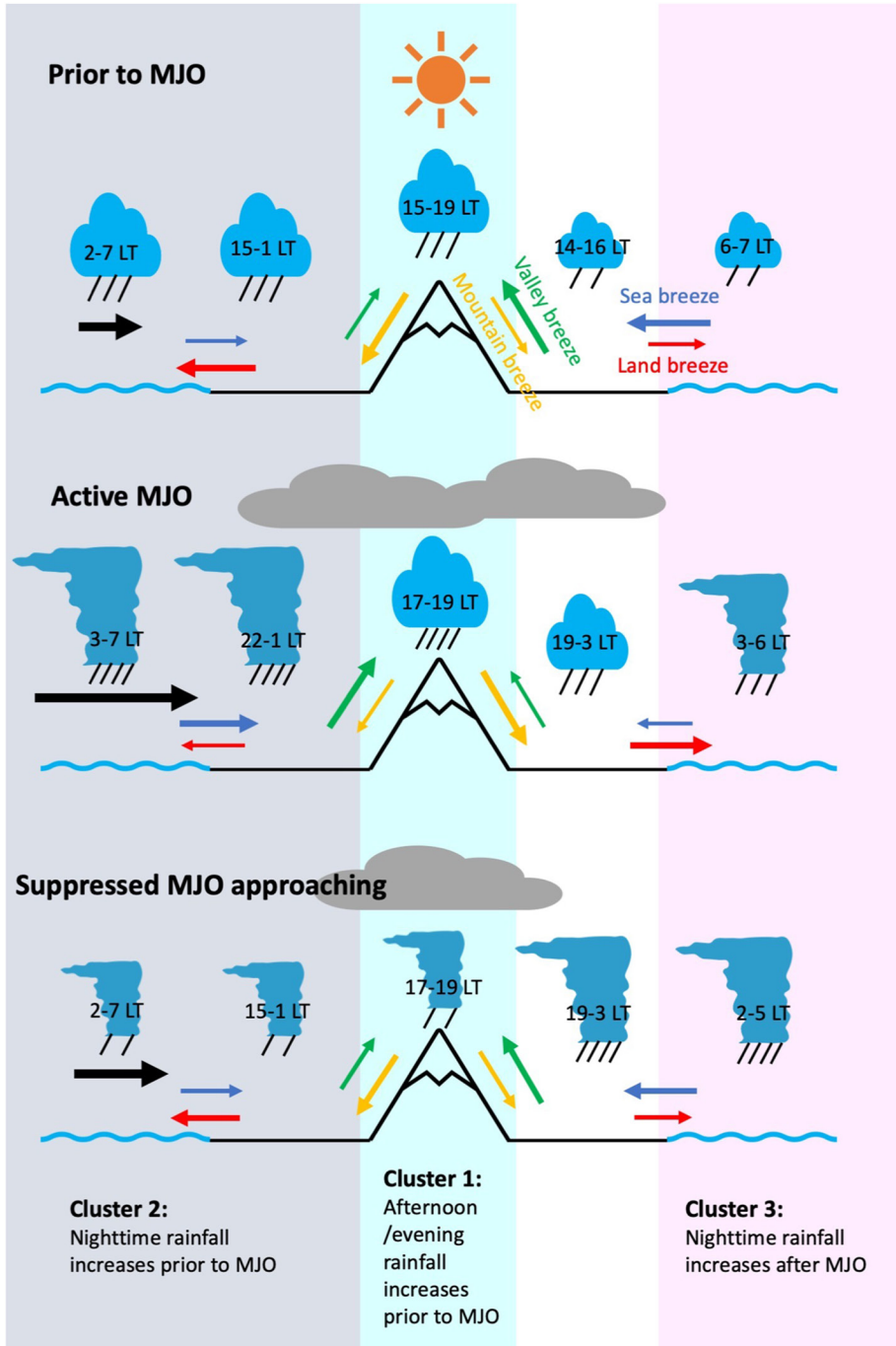

Figure 13. Schematic of the Maritime Continent diurnal rainfall changes with the passage of the Madden-Julian Oscillation (MJO), summarizing Figures 3, 4, and 7–9. The upper, middle and lower panels represent conditions prior to, during and after the active MJO, respectively. Blue/red/green/orange arrows indicate sea/land/valley/mountain breeze, respectively. Blue clouds indicate local rainfall, with local time representing the approximate time range of the primary diurnal peak. Clouds with an anvil represent precipitation with more of a stratiform component. Size of the arrows/clouds shows variations in the magnitude of breezes/rainfall between panels, but do not differentiate magnitudes within one panel. Thick black arrows indicate the low-level large-scale wind induced by the MJO. Background colors indicate regions grouped into the three clusters in Figure 9.

based on TRMM/GPM PR data, the vanguard precipitation anomalies over land ahead of the main body MJO consist of mostly convective rain. Stratiform rain fraction increases over low-elevation land regions to the west of orography and offshore regions during the active MJO and stratiform rain dominates the region (including the rearguard precipitation over land) as the suppressed MJO approaches the MC.

Influences of moisture and winds associated with the MJO on rainfall anomalies were further investigated using ERA5 reanalysis. The diurnal rainfall anomalies in Figure 7 closely follow the daily rainfall anomalies in Figure 3, because when the daily mean increases, the peak of the diurnal rainfall is also enhanced with the passage of the MJO (Figure 8). Therefore, the question of what determines the east-west asymmetry in daily and diurnal rainfall anomalies related to topography reduces to what determines the daily rainfall anomalies. Our main findings concerning MJO-induced environmental changes can be summarized as follows:

Moisture convergence of the low-frequency moisture by the MJO anomalous winds dominates the anomalous MFC, thus the anomalous daily rainfall. Moisture advection of the low-frequency moisture by the MJO anomalous winds also modifies the anomalous MFC. This suggests the importance of low-frequency moisture and anomalous MJO winds to the MC diurnal rainfall, implying that variations in MJO moisture may not play a big role in the rainfall asymmetry around topography. The lesser importance of MJO-scale moisture may be due to its smaller variation compared to climatology. The east-west asymmetry related to topography is caused by the horizontal MJO wind being intercepted by the topography, leading to a discontinuous wind gradient on either side of the mountains and thus asymmetry in divergence, which further leads to asymmetry in MJO vertical velocity. While previous studies reported that the diurnal wind may be important to determine the diurnal rainfall anomalies over the MC during the MJO, our analysis indicates that the east-west topographic rainfall asymmetry (daily and diurnal) may not be associated with diurnal variations in moisture or wind, but rather longer temporal scale variations. The daily/diurnal rainfall over most of the open ocean areas near the MC is insignificantly correlated with MJO-induced winds, indicating MJO wind modulation is closely linked to the MC topography/land.

This study highlights the role of mountains in modulating the impacts of the MJO on the daily and diurnal rain over the MC, and thus the importance of accurately representing topographic effects in numerical models. However, open questions remain to be answered. For example, high terrain and wind shear can further complicate wind modulation of the diurnal rainfall over the islands, whose relationship should be quantified by further modeling work.

Data Availability Statement

The TRMM/GPM IMERG and PR/DPR data were provided by the NASA/Goddard Space Flight Center's Precipitation Processing Center. The datasets are archived at the NASA GES DISC (https://disc.gsfc.nasa.gov). All ERA5 fields analyzed in this study are openly available from the Copernicus Climate Change Service (C3S) Climate Data Store (https://cds.climate.copernicus.eu/).

Acknowledgments
This research was supported by NOAA Climate Variability and Predictability Program, under grant NA17OAR4310258. We thank Aaron Funk for processing the PR/DPR data.

References

Adames, Á. F., & Kim, D. (2016). The MJO as a dispersive, convectively coupled moisture wave: Theory and observations. *Journal of the Atmospheric Sciences*, *73*(3), 913–941. https://doi.org/10.1175/jas-d-15-0170.1

Ahn, M.-S., Kim, D., Ham, Y.-G., & Park, S. (2020). Role of Maritime Continent land convection on the mean state and MJO propagation. *Journal of Climate*, *33*(5), 1659–1675. https://doi.org/10.1175/jcli-d-19-0342.1

Arulraj, M., & Barros, A. P. (2021). Automatic detection and classification of low-level orographic precipitation processes from space-borne radars using machine learning. *Remote Sensing of Environment*, *257*, 112355. https://doi.org/10.1016/j.rse.2021.112355

Bai, H., Deranadyan, G., Schumacher, C., Funk, A., Epifanio, C., Ali, A., et al. (2021). Formation of nocturnal offshore rainfall near the west coast of Sumatra: Land breeze or gravity wave? *Monthly Weather Review*, *149*(3), 715–731. https://doi.org/10.1175/mwr-d-20-0179.1

Barnes, H. C., Zuluaga, M. D., & Houze, R. A., Jr. (2015). Latent heating characteristics of the mjo computed from trmm observations. *Journal of Geophysical Research: Atmospheres*, *120*(4), 1322–1334. https://doi.org/10.1002/2014jd022530

Biasutti, M., Yuter, S. E., Burleyson, S. D., & Sobel, A. H. (2012). Very high resolution rainfall patterns measured by TRMM precipitation radar: Seasonal and diurnal cycles. *Climate Dynamics*, *39*(1–2), 239–258. https://doi.org/10.1007/s00382-011-1146-6

Birch, C., Webster, S., Peatman, S., Parker, D., Matthews, A., Li, Y., & Hassim, M. (2016). Scale interactions between the MJO and the western Maritime Continent. *Journal of Climate*, *29*(7), 2471–2492. https://doi.org/10.1175/jcli-d-15-0557.1

Burpee, R. W., & Lahiffi, L. N. (1984). Area-average rainfall variations on sea-breeze days in south Florida. *Monthly Weather Review*, *112*(3), 520–534. https://doi.org/10.1175/1520-0493(1984)112<0520:aarvos>2.0.co;2

Carbone, R., & Tuttle, J. (2008). Rainfall occurrence in the US warm season: The diurnal cycle. *Journal of Climate*, *21*(16), 4132–4146. https://doi.org/10.1175/2008jcli2275.1

Dai, A., Giorgi, F., & Trenberth, K. E. (1999). Observed and model-simulated diurnal cycles of precipitation over the contiguous United States. *Journal of Geophysical Research*, *104*(D6), 6377–6402. https://doi.org/10.1029/98jd02720

Da Silva, N. A., & Matthews, A. J. (2021). Impact of the Madden–Julian Oscillation on extreme precipitation over the western Maritime Continent and Southeast Asia. *Quarterly Journal of the Royal Meteorological Society*, *147*(739), 3434–3453. https://doi.org/10.1002/qj.4136

DeMott, C. A., Wolding, B. O., Maloney, E. D., & Randall, D. A. (2018). Atmospheric mechanisms for MJO decay over the Maritime Continent. *Journal of Geophysical Research: Atmospheres*, *123*(10), 5188–5204. https://doi.org/10.1029/2017jd026979

de Szoeke, S. P., Edson, J. B., Marion, J. R., Fairall, C. W., & Bariteau, L. (2015). The MJO and air–sea interaction in TOGA COARE and DYNAMO. *Journal of Climate*, *28*(2), 597–622. https://doi.org/10.1175/jcli-d-14-00477.1

Du, Y., & Rotunno, R. (2018). Diurnal cycle of rainfall and winds near the south coast of China. *Journal of the Atmospheric Sciences*, *75*(6), 2065–2082. https://doi.org/10.1175/jas-d-17-0397.1

Du, Y., Rotunno, R., & Zhang, F. (2019). Impact of vertical wind shear on gravity wave propagation in the land-sea breeze circulation at the equator. *Journal of the Atmospheric Sciences*, *76*, 3247–3265. https://doi.org/10.1175/jas-d-19-0069.1

Duan, Y., Wilson, A. M., & Barros, A. P. (2015). Scoping a field experiment: Error diagnostics of TRMM precipitation radar estimates in complex terrain as a basis for IPHEx2014. *Hydrology and Earth System Sciences*, *19*(3), 1501–1520. https://doi.org/10.5194/hess-19-1501-2015

Gray, W. M., & Jacobson, R. W. (1977). Diurnal variation of deep cumulus convection. *Monthly Weather Review*, *105*(9), 1171–1188. https://doi.org/10.1175/1520-0493(1977)105<1171:dvodcc>2.0.co;2

Hagos, S. M., Zhang, C., Feng, Z., Burleyson, C. D., De Mott, C., Kerns, B., & Martini, M. N. (2016). The impact of the diurnal cycle on the propagation of Madden-Julian Oscillation convection across the Maritime Continent. *Journal of Advances in Modeling Earth Systems*, *8*(4), 1552–1564. https://doi.org/10.1002/2016ms000725

Hersbach, H., Bell, B., Berrisford, P., Hirahara, S., Horányi, A., Muñoz-Sabater, J., et al. (2020). The ERA5 global reanalysis. *Quarterly Journal of the Royal Meteorological Society*, *146*(730), 1999–2049. https://doi.org/10.1002/qj.3803

Hirose, M., Oki, R., Shimizu, S., Kachi, M., & Higashiuwatoko, T. (2008). Finescale diurnal rainfall statistics refined from eight years of TRMM PR data. *Journal of Applied Meteorology and Climatology*, *47*(2), 544–561. https://doi.org/10.1175/2007jamc1559.1

Houze, R. A. (2012). Orographic effects on precipitating clouds. *Reviews of Geophysics*, *50*(1), RG1001. https://doi.org/10.1029/2011rg000365

Houze, R. A., Geotis, S. G., Marks, F. D., Jr, & West, A. K. (1981). Winter monsoon convection in the vicinity of north Borneo. Part I: Structure and time variation of the clouds and precipitation. *Monthly Weather Review*, *109*, 1595–1614. https://doi.org/10.1175/1520-0493(1981)109<1595:wmcitv>2.0.co;2

Huffman, G. J., Bolvin, D. T., Braithwaite, D., Hsu, K., Joyce, R., Xie, P., & Yoo, S.-H. (2015). NASA global precipitation measurement (GPM) integrated multi-satellite retrievals for GPM (IMERG). *Algorithm Theoretical Basis Document (ATBD) Version*, *4*, 26.

Ichikawa, H., & Yasunari, T. (2007). Propagating diurnal disturbances embedded in the Madden-Julian Oscillation. *Geophysical Research Letters*, *34*(18), L18811. https://doi.org/10.1029/2007gl030480

Iguchi, T. (2020). Dual-frequency precipitation radar (DPR) on the global precipitation measurement. *Satellite Precipitation Measurement: Volume 1*, *67*, 183. https://doi.org/10.1007/978-3-030-24568-9_11

Inness, P. M., & Slingo, J. M. (2006). The interaction of the Madden–Julian oscillation with the Maritime Continent in a GCM. *Quarterly Journal of the Royal Meteorological Society*, *132*(618), 1645–1667. https://doi.org/10.1256/qj.05.102

Jiang, X., Adames, Á. F., Kim, D., Maloney, E. D., Lin, H., Kim, H., & Klingaman, N. P. (2020). Fifty years of research on the Madden-Julian Oscillation: Recent progress, challenges, and perspectives. *Journal of Geophysical Research: Atmospheres*, *125*(17), e2019JD030911. https://doi.org/10.1029/2019jd030911

Jiang, X., Su, H., & Waliser, D. E. (2019). A damping effect of the Maritime Continent for the Madden-Julian oscillation. *Journal of Geophysical Research: Atmospheres*, *124*(24), 13693–13713. https://doi.org/10.1029/2019jd031503

Johnson, R. H., & Ciesielski, P. E. (2013). Structure and properties of Madden–Julian oscillations deduced from DYNAMO sounding arrays. *Journal of the Atmospheric Sciences*, *70*(10), 3157–3179. https://doi.org/10.1175/jas-d-13-065.1

Kikuchi, K., & Wang, B. (2008). Diurnal precipitation regimes in the global tropics. *Journal of Climate*, *21*(11), 2680–2696. https://doi.org/10.1175/2007jcli2051.1

Kiladis, G. N., Straub, K. H., & Haertel, P. T. (2005). Zonal and vertical structure of the Madden–Julian oscillation. *Journal of the Atmospheric Sciences*, *62*(8), 2790–2809. https://doi.org/10.1175/jas3520.1

Kousky, V. E. (1980). Diurnal rainfall variation in northeast Brazil. *Monthly Weather Review*, *108*(4), 488–498. https://doi.org/10.1175/1520-0493(1980)108<0488:drvinb>2.0.co;2

Ling, J., Zhang, C., Joyce, R., Xie, P.-p., & Chen, G. (2019). Possible role of the diurnal cycle in land convection in the barrier effect on the MJO by the Maritime Continent. *Geophysical Research Letters*, *46*(5), 3001–3011. https://doi.org/10.1029/2019gl081962

Lu, J., Li, T., & Wang, L. (2019). Precipitation diurnal cycle over the Maritime Continent modulated by the MJO. *Climate Dynamics*, *53*(9), 6489–6501. https://doi.org/10.1007/s00382-019-04941-8

Madden, R. A., & Julian, P. R. (1972). Description of global-scale circulation cells in the tropics with a 40–50 day period. *Journal of the Atmospheric Sciences*, *29*, 1109–1123. https://doi.org/10.1175/1520-0469(1972)029<1109:dogscc>2.0.co;2

Mapes, B. E., Warner, T. T., Xu, M., & Negri, A. J. (2003). Diurnal patterns of rainfall in northwestern South America. Part I: Observations and context. *Monthly Weather Review*, *131*(5), 799–812. https://doi.org/10.1175/1520-0493(2003)131<0799:dporin>2.0.co;2

McPhaden, M. J., Zhang, X., Hendon, H. H., & Wheeler, M. C. (2006). Large scale dynamics and MJO forcing of ENSO variability. *Geophysical Research Letters*, *33*(16), L16702. https://doi.org/10.1029/2006gl026786

Mori, S., Hamada, J. I., Tauhid, Y. I., Yamanaka, M. D., Okamoto, N., Murata, F., et al. (2004). Diurnal land–sea rainfall peak migration over Sumatera Island, Indonesian Maritime Continent, observed by TRMM satellite and intensive rawinsonde soundings. *Monthly Weather Review*, *132*(8), 2021–2039. https://doi.org/10.1175/1520-0493(2004)132<2021:dlrpmo>2.0.co;2

Natoli, M. B., & Maloney, E. D. (2019). Intraseasonal variability of the diurnal cycle of precipitation in the Philippines. *Journal of the Atmospheric Sciences*, *76*(11), 3633–3654. https://doi.org/10.1175/jas-d-19-0152.1

Nesbitt, S. W., & Zipser, E. J. (2003). The diurnal cycle of rainfall and convective intensity according to three years of TRMM measurements. *Journal of Climate*, *16*(10), 1456–1475. https://doi.org/10.1175/1520-0442-16.10.1456

Peatman, S. C., Matthews, A. J., & Stevens, D. P. (2014). Propagation of the Madden–Julian Oscillation through the Maritime Continent and scale interaction with the diurnal cycle of precipitation. *Quarterly Journal of the Royal Meteorological Society*, *140*(680), 814–825. https://doi.org/10.1002/qj.2161

Qian, J.-H. (2020). Mechanisms for the dipolar patterns of rainfall variability over large islands in the Maritime Continent associated with the Madden–Julian oscillation. *Journal of the Atmospheric Sciences*, *77*(6), 2257–2278. https://doi.org/10.1175/jas-d-19-0091.1

Rauniyar, S. P., & Walsh, K. J. (2011). Scale interaction of the diurnal cycle of rainfall over the Maritime Continent and Australia: Influence of the MJO. *Journal of Climate*, *24*(2), 325–348. https://doi.org/10.1175/2010jcli3673.1

Sakaeda, N., Kiladis, G., & Dias, J. (2020). The diurnal cycle of rainfall and the convectively coupled equatorial waves over the Maritime Continent. *Journal of Climate*, *33*(8), 3307–3331. https://doi.org/10.1175/jcli-d-19-0043.1

Sakurai, N., Murata, F., Yamanaka, M. D., Mori, S., Hamada, J.-I., Hashiguchi, H., et al. (2005). Diurnal cycle of cloud system migration over Sumatera Island. *Journal of the Meteorological Society of Japan*, *83*(5), 835–850. https://doi.org/10.2151/jmsj.83.835

Schumacher, C., & Houze, R. A. (2003). Stratiform rain in the tropics as seen by the TRMM precipitation radar. *Journal of Climate*, *16*(11), 1739–1756. https://doi.org/10.1175/1520-0442(2003)016<1739:sritta>2.0.co;2

Seiki, A., Yokoi, S., & Katsumata, M. (2021). The impact of diurnal precipitation over Sumatra Island, Indonesia, on synoptic disturbances and its relation to the Madden-Julian Oscillation. *Journal of the Meteorological Society of Japan*, *99*, 113–137. https://doi.org/10.2151/jmsj.2021-007

Short, E., Vincent, C. L., & Lane, T. P. (2019). Diurnal cycle of surface winds in the Maritime Continent observed through satellite scatterometry. *Monthly Weather Review*, *147*(6), 2023–2044. https://doi.org/10.1175/mwr-d-18-0433.1

Sobel, A. H., Maloney, E. D., Bellon, G., & Frierson, D. M. (2010). Surface fluxes and tropical intraseasonal variability: A reassessment. *Journal of Advances in Modeling Earth Systems*, *2*(1), 27. https://doi.org/10.3894/james.2010.2.2

Stan, C., Straus, D. M., Frederiksen, J. S., Lin, H., Maloney, E. D., & Schumacher, C. (2017). Review of tropical-extratropical teleconnections on intraseasonal time scales. *Reviews of Geophysics*, *55*(4), 902–937. https://doi.org/10.1002/2016rg000538

Thorndike, R. L. (1953). Who belongs in the family? *Psychometrika*, *18*(4), 267–276. https://doi.org/10.1007/bf02289263

Tian, B. J., Waliser, D. E., & Fetzer, E. J. (2006). Modulation of the diurnal cycle of tropical deep convective clouds by the MJO. *Geophysical Research Letters*, *33*(20), L20704. https://doi.org/10.1029/2006gl027752

Virts, K. S., & Houze, R. A. (2015). Variation of lightning and convective rain fraction in mesoscale convective systems of the MJO. *Journal of the Atmospheric Sciences*, *72*(5), 1932–1944. https://doi.org/10.1175/jas-d-14-0201.1

Wang, S., & Sobel, A. H. (2017). Factors controlling rain on small tropical islands: Diurnal cycle, large-scale wind speed, and topography. *Journal of the Atmospheric Sciences*, *74*(11), 3515–3532. https://doi.org/10.1175/jas-d-16-0344.1

Wheeler, M. C., & Hendon, H. H. (2004). An all-season real-time multivariate MJO index: Development of an index for monitoring and prediction. *Monthly Weather Review*, *132*(8), 1917–1932. https://doi.org/10.1175/1520-0493(2004)132<1917:aarmmi>2.0.co;2

Wu, C.-H., & Hsu, H.-H. (2009). Topographic influence on the MJO in the Maritime Continent. *Journal of Climate*, *22*(20), 5433–5448. https://doi.org/10.1175/2009jcli2825.1

Yang, G. Y., & Slingo, J. (2001). The diurnal cycle in the tropics. *Monthly Weather Review*, *129*(4), 784–801. https://doi.org/10.1175/1520-0493(2001)129<0784:tdcitt>2.0.co;2

Yokoi, S., Mori, S., Syamsudin, F., Haryoko, U., & Geng, B. (2019). Environmental conditions for nighttime offshore migration of precipitation area as revealed by in situ observation off Sumatra Island. *Monthly Weather Review*, *147*(9), 3391–3407. https://doi.org/10.1175/mwr-d-18-0412.1

Yuter, S. E., & Houze, R. A. (1998). The natural variability of precipitating clouds over the western Pacific warm pool. *Quarterly Journal of the Royal Meteorological Society*, *124*(545), 53–99. https://doi.org/10.1002/qj.49712454504

Zhang, C. (2005). Madden-Julian Oscillation. *Reviews of Geophysics*, *43*(2), RG2003. https://doi.org/10.1029/2004rg000158

Zhang, C. (2013). Madden–Julian oscillation: Bridging weather and climate. *Bulletin of the American Meteorological Society*, *94*(12), 1849–1870. https://doi.org/10.1175/bams-d-12-00026.1

Zhang, C., & Ling, J. (2017). Barrier effect of the Indo-Pacific Maritime Continent on the MJO: Perspectives from tracking MJO precipitation. *Journal of Climate*, *30*(9), 3439–3459. https://doi.org/10.1175/jcli-d-16-0614.1

Zhang, C., Ling, J., Hagos, S., Tao, W.-K., Lang, S., Takayabu, Y. N., & L'Ecuyer, T. (2010). MJO signals in latent heating: Results from TRMM retrievals. *Journal of the Atmospheric Sciences*, *67*(11), 3488–3508. https://doi.org/10.1175/2010jas3398.1

Zhou, W., Yang, D., Xie, S.-P., & Ma, J. (2020). Amplified Madden–Julian oscillation impacts in the Pacific–North America region. *Nature Climate Change*, *10*(7), 654–660. https://doi.org/10.1038/s41558-020-0814-0